Optimizing a Protocol for Fluorescence Recovery After Photobleaching Experiments

Sarafa Adewale Iyaniwura (iyaniwura@aims.ac.za)
African Institute for Mathematical Sciences (AIMS)

Supervised by: Professor Daniel Coombs
The University of British Columbia, Canada

22 May 2014

Submitted in partial fulfillment of a structured masters degree at AIMS South Africa

Abstract

Fluorescence Recovery After Photobleaching (FRAP) is a technique for estimating the mobility of fluorescently tagged molecules in living cells. The most widely used tool for FRAP experiments is the Confocal Laser Scanning Microscope (CLSM) which allows the bleaching of arbitrary regions. During FRAP experiments with the CLSM, there is usually a trade-off between the time-step at which data are acquired and the size of the observation region. In this project, we developed several one-dimensional and two-dimensional models for analysing FRAP data. We used these models to simulate FRAP recovery curves and then used the least square method to estimate the diffusion coefficient from the data generated. In addition to this, we provided the optimal locations in the bleached region and the optimal timing for acquiring data during FRAP experiments in order to reduce the effect of the trade-off on the accuracy of the data acquired.

Declaration

I, the undersigned, hereby declare that the work contained in this research project is my original work, and that any work done by others or by myself previously has been acknowledged and referenced accordingly.

Sarafa Adewale Iyaniwura, 22 May 2014

Contents

1. Introduction

1.1 Fluorescence recovery after photobleaching

Fluorescence Recovery After Photobleaching (FRAP) is a technique for studying the mobility of molecules in different media such as living cells. It was developed 40 years ago and was first used to study the lateral diffusion of proteins and lipids in cell membranes. Lateral diffusion in cell membranes is well-established and varies according to the physiological state of living cells (Axelrod et al., 1976).

Photobleaching occurs when there is an irreversible breakdown of fluorescence in fluorophores as a result of exposure to high intensity laser stimulation by wave lengths close to the excitation peak of the fluorophores. FRAP involves the bleaching of fluorescence in a small region of a surface containing fluorescent molecules, and then monitoring the random movement of molecules in and out of the bleached region. This movement increases the fluorescence intensity inside the bleached region until an equilibrium level of intensity is reached (Braga et al., 2004).

The classical method for FRAP experiments involved the use of non-scanning microscopes where bleaching is performed with a stationary laser beam that is focused on the samples. Nowadays, the most commonly used tool for performing FRAP experiments is the Confocal Laser Scanning Microscope (CLSM) which is equipped with features such as acoustic-optic tunable filter (AOTF) that enables the bleaching of arbitrary regions in the sample. This feature makes the CLSM an excellent tool for performing FRAP experiments. When using CLSM, the region to be bleached, the pattern and degree of bleaching are specified in the software, after which the microscope scans the laser beam over the region in a sequential pattern point-by-point and line-by-line, while modulating the intensity of the beam according to the specified pattern (Braeckmans et al., 2003). The CLSM uses its laser to acquire images at low-intensity and for bleaching at high-intensity.

In a typical FRAP experiment to determine the mobility of specific proteins on a living cell surface, the protein of interest is fluorescently tagged. Images of the labelled protein are acquired at low-laser intensity in order to determine its pre-bleach fluorescent intensity. Next, high-laser intensity is used to bleach a small region of the cell surface for a short time. This region is referred to as the region of interest (ROI). After the bleaching, images of the fluorescence recovery process in the bleached region are acquired at low-laser intensity and at specified time-steps. The total time of the experiment depends on the observed rate of recovery. The higher the mobility of the labelled protein, the shorter the recovery time and thus, the shorter the time of the experiment.

The data obtained from FRAP experiments can be used to estimate the diffusion coefficient of the labelled proteins, and the percentage of proteins that are immobile. The average diffusivity of the protein is represented by the intensity of the recovered fluorescence. The form of recovery depends on factors such as the mobility of the labelled protein, the size and shape of the region of interest, and the amount of bleaching.

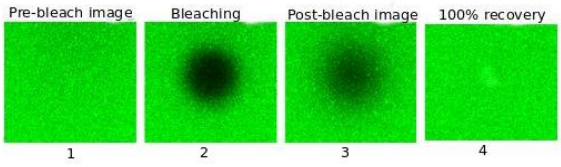

Figure 1.1: FRAP experiment with 100% recovery.

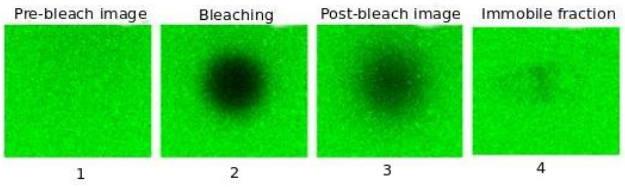

Figure 1.2: FRAP experiment with immobile fraction.

Figure 1.1 and 1.2 give a pictorial description of a typical FRAP experiment. Figure 1.1 involves a situation where all the proteins in the bleached region are able to move out of the region thereby leading to 100% recovery while in Figure 1.2 we have a fraction of the protein that are unable to diffuse out of the bleached region leading to the remaining darker spot in the fourth image of the figure.

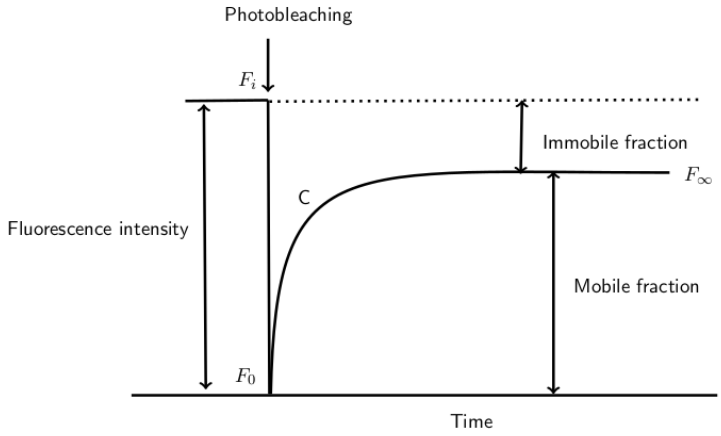

Figure 1.3: Recovery curve of FRAP experiment.

Figure 1.3 is the graphical representation of a typical data obtained from an ideal FRAP experiment. In this figure, F_i is the fluorescence intensity before photobleaching, F_0 is the fluorescence intensity immediately after photobleaching and F_∞ is the fluorescence intensity after a long recovery time. The slope of the curve is determined by the diffusivity of the labelled protein. The steeper the slope, the faster the recovery and thus, the higher the diffusion coefficient.

There are technical problems encountered when using the CLSM for FRAP experiments. First, the laser take a long time to bleach a rectangular strip. As a result of this, recovery may have started in some parts of the bleached region while bleaching is going on at other parts. There is a trade-off between the speed of data acquisition and the size of the bleached region. In addition, the low-laser intensity used for data acquisition causes background bleaching which may affect the accuracy of the data acquired.

In this research project, we developed one-dimensional and two-dimensional models for analysing FRAP data considering different bleach spots. We used these models to simulate FRAP data and then used the least square method to estimate the diffusion coefficient from the simulated data. We aimed at optimizing the locations in the bleached region and the timing for data acquisition in FRAP experiments in order to estimate the protein's diffusion coefficient as accurately as possible.

1.2 Diffusion coefficient

Diffusion from a molecular point of view, is based on the thermal motion of particles such as liquid and gas at temperatures above the absolute zero temperature, and describes the net flux of molecules from a region of high concentration to a region of low concentration. Diffusion is of great importance in disciplines such as chemistry, physics and biology. An important application of diffusion in cell biology is in the transport of materials, e.g the transport of amino acids within cells.

The diffusion coefficient of a substance is the rate at which a mass of the substance diffuses through a unit time at a concentration gradient of unity . It indicates the diffusional mobility of a substance and depends on some properties of the substance such as the sizes of its molecules among others. The higher the diffusion coefficient of a substance, the higher its diffusional mobility.

1.3 Mobile and Immobile fraction

In a FRAP experiment, it is expected that there will be fluorescence recovery in the bleached region. However, it is often difficult to have 100% fluorescence recovery after bleaching. This is as a result of some molecules in the bleached region that are unable to move out of the region. The fraction of these molecules is known as the immobile fraction. On the other hand, the fraction of the molecules that are able to diffuse out of the bleached region is known as the mobile fraction and it is defined as

$$M_f = \frac{F_\infty - F_0}{F_i - F_0} \tag{1.3.1}$$

where F_∞, F_i, and F_0 are as defined in Figure 1.1. Thus, the immobile fraction is $1 - M_f$.

1.4 Least square method

The Least square method is a popular technique in statistics for data fitting. It is widely used to estimate the numerical values of the parameters used to fit a function to a set of data. The least square method is categorised into two: the ordinary or linear least squares and the non-linear least squares. In this project, we used the ordinary least square method for estimating the diffusion coefficient from FRAP data. This method involves minimizing the sum of squared difference over a set of possible values of the diffusion coefficient. It is given as

$$ssd(D) = \sum_{i=1}^{N} [d_i - (1-f)H(D, t_i)]^2 \tag{1.4.1}$$

where D is a possible values of the diffusion coefficient, f is the immobile fraction, N is the number of data points, d_i are the FRAP data, and $H(D, t_i)$ are the intensity values from the model.

2. Model Derivation

In this chapter, we derive several Partial Differential Equations (PDEs) to model the fluorescence intensity in the bleached region of a cell during FRAP experiment. These PDEs vary in dimension and depend on the geometry of the bleach region under consideration in the experiment. The equations were solved using different methods and with FRAP like initial conditions. We then integrate the solutions of these equations over the entire bleached region to get a function which can be used to predict the fluorescence intensity in the bleached region.

2.1 Derivation of the one-dimensional models

We begin by deriving the one-dimensional models which are used to model the bleaching of a rectangular strip. These models are developed by using the one-dimensional diffusion equation,

$$\frac{1}{D}\frac{\partial f(x,t)}{\partial t} = \frac{\partial^2 f(x,t)}{\partial x^2} \tag{2.1.1}$$

where $f(x,t)$ is the fluorescence intensity at position x and time t, and D is the diffusion coefficient.

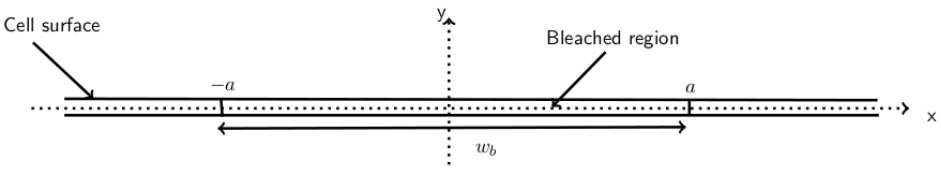

Figure 2.1: A rectangular strip bleach.

We developed these models using two different approaches which are the Fourier transforms and Fourier series approach.

2.1.1 Fourier transform approach. This approach involves using the Fourier transforms in solving Equation (2.1.1). In this approach, we assumed that the rectangular strip is infinite and that the bleached region has a width w_b ($[-a,a]$). We also assumed that the initial fluorescent intensity everywhere on the strip is unity except in the bleached region where the intensity is zero. This initial condition can be written as

$$f(x,0) = \phi(x) = \begin{cases} 0, & -a \le x \le a \\ 1, & \text{otherwise.} \end{cases} \tag{2.1.2}$$

First, let us define the Fourier transform of $f(x,t)$ as

$$\mathscr{F}\left[f(x,t)\right] = \tilde{f}(k,t) = \int_{-\infty}^{\infty} f(x,t)e^{-ikx}\,\mathrm{d}x\ , \tag{2.1.3}$$

Then from Equation (2.1.1), we have

$$\int_{-\infty}^{\infty} \frac{\partial f}{\partial t}e^{-ikx}\,\mathrm{d}x = D\int_{-\infty}^{\infty} \frac{\partial^2 f}{\partial x^2}e^{-ikx}\,\mathrm{d}x$$

$$\frac{\partial \tilde{f}}{\partial t} = -Dk^2\tilde{f}\ . \tag{2.1.4}$$

Also, taking the Fourier transform of the initial condition, we obtain

$$\tilde{f}(k,0) = \tilde{\phi}(k) \ . \tag{2.1.5}$$

We solved Equation (2.1.4), to get

$$\tilde{f}(k,t) = Ae^{-Dk^2t} \qquad (A \text{ is a constant}) \tag{2.1.6}$$

and then we apply the initial condition in Equation (2.1.5) to the solution in Equation (2.1.6),

$$\tilde{f}(k,t) = \tilde{\phi}(k)e^{-Dk^2t} \ . \tag{2.1.7}$$

From the products and convolution properties of Fourier transforms,

$$\mathscr{F}\left[h * g\right] = \mathscr{F}\left[h\right] \cdot \mathscr{F}\left[g\right] = \tilde{h} \cdot \tilde{g} \tag{2.1.8}$$

where

$$(h * g)(x) = \int_{-\infty}^{\infty} h(\zeta)g(x-\zeta)\,\mathrm{d}\zeta \ . \tag{2.1.9}$$

Also, we know that

$$\mathscr{F}\left[\frac{e^{-\frac{x^2}{a^2}}}{a\sqrt{\pi}}\right] = e^{-\frac{k^2a^2}{4}} \ .$$

If we let $a^2/4 = Dt$, then $a = \sqrt{4Dt}$ and so,

$$\mathscr{F}\left[\frac{e^{-\frac{x^2}{4Dt}}}{\sqrt{4Dt\pi}}\right] = e^{-Dk^2t} \ . \tag{2.1.10}$$

Now, applying Equations (2.1.8), (2.1.9) and (2.1.10) to Equation (2.1.7), we have

$$f(x,t) = \int_{-\infty}^{\infty} \phi(\zeta) \left(\frac{e^{-\frac{(x-\zeta)^2}{4Dt}}}{\sqrt{4Dt\pi}}\right) \mathrm{d}\zeta \ ,$$

$$f(x,t) = \frac{1}{\sqrt{4Dt\pi}} \int_{-\infty}^{\infty} \phi(\zeta) e^{\frac{-(x-\zeta)^2}{4Dt}}\,\mathrm{d}\zeta \ , \tag{2.1.11}$$

Applying the initial condition in Equation (2.1.2) to Equation (2.1.11), we obtained

$$f(x,t) = \int_{-\infty}^{-a} \frac{e^{-\frac{(x-\zeta)^2}{4Dt}}}{\sqrt{4Dt\pi}}\,\mathrm{d}\zeta + \int_{a}^{\infty} \frac{e^{-\frac{(x-\zeta)^2}{4Dt}}}{\sqrt{4Dt\pi}}\,\mathrm{d}\zeta \ . \tag{2.1.12}$$

If we let $\frac{(\zeta-x)}{\sqrt{4Dt}} = s$, then $\mathrm{d}\zeta = \sqrt{4Dt}\ \mathrm{d}s$. Substituting for s in Equation (2.1.12), we have

$$f(x,t) = \frac{1}{\sqrt{\pi}} \int_{-\infty}^{\frac{-(a+x)}{\sqrt{4Dt}}} e^{-s^2}\,\mathrm{d}s + \frac{1}{\sqrt{\pi}} \int_{\frac{(a-x)}{\sqrt{4Dt}}}^{\infty} e^{-s^2}\,\mathrm{d}s \ ,$$

and since

$$\frac{1}{\sqrt{\pi}}\int_{-\infty}^{\infty} e^{-s^2}\,\mathrm{d}s = 1\ ,$$

it follows that

$$f(x,t) = \left(1 - \frac{1}{\sqrt{\pi}}\int_{\frac{-(a+x)}{\sqrt{4Dt}}}^{\infty} e^{-s^2}\,\mathrm{d}s\right) + \frac{1}{\sqrt{\pi}}\int_{\frac{(a-x)}{\sqrt{4Dt}}}^{\infty} e^{-s^2}\,\mathrm{d}s$$

$$= 1 - \frac{1}{2}\,\mathrm{erfc}\left(\frac{-(a+x)}{\sqrt{4Dt}}\right) + \frac{1}{2}\,\mathrm{erfc}\left(\frac{a-x}{\sqrt{4Dt}}\right)$$

$$= 1 - \frac{1}{2}\left(1 + \mathrm{erf}\left(\frac{a+x}{\sqrt{4Dt}}\right)\right) + \frac{1}{2}\left(1 - \mathrm{erf}\left(\frac{a-x}{\sqrt{4Dt}}\right)\right)\ .$$

Simplifying, we obtain

$$f(x,t) = 1 - \frac{1}{2}\mathrm{erf}\left(\frac{a+x}{\sqrt{4Dt}}\right) - \frac{1}{2}\mathrm{erf}\left(\frac{a-x}{\sqrt{4Dt}}\right) \tag{2.1.13}$$

where erf is the usual error function.

This is the solution of the diffusion equation in Equation (2.1.1) with respect to our initial condition.

Next, we integrate the function $f(x,t)$ as defined in Equation (2.1.13) over the entire bleached region to get

$$H(t,D) = \frac{2\sqrt{Dt}}{\sqrt{\pi}}\left[1 - \exp\left(\frac{-a^2}{Dt}\right)\right] + 2a\left[\mathrm{erf}\left(\frac{a}{\sqrt{Dt}}\right) - 1\right]\ .$$

Since $w_b = 2a$, we have

$$H(t,D) = \frac{2\sqrt{Dt}}{\sqrt{\pi}}\left[1 - \exp\left(\frac{-w_b^2}{4Dt}\right)\right] + w_b\left[\mathrm{erf}\left(\frac{w_b}{2\sqrt{Dt}}\right) - 1\right] \tag{2.1.14}$$

where w_b is the width of the bleach region and D is the diffusion coefficient of the proteins.

This is the model for the Fourier transforms approach.

2.1.2 Fourier Series approach. In this approach, we used separation of variables and Fourier series method to solve the diffusion equation in Equation (2.1.1). Here, we assumed that the rectangular strip is of finite length $L_c = 2L$ $([-L, L])$ and the bleached region is of width $w_b = 2a$ $([-a, a] \subset [-L, L])$. In developing this model, we also assumed that the boundaries of the strip satisfy the Neumann boundary conditions below.

$$f_x(-L,t) = f_x(L,t) = 0\ . \tag{2.1.15}$$

We begin by using the method of separation of variable. Let

$$f(x,t) = X(x)T(t)\ .$$

Then Equation (2.1.1) becomes,

$$\frac{1}{D}X(x)T'(t) = X''(x)T(t)$$
$$\frac{1}{D}\frac{T'(t)}{T(t)} = \frac{X''(x)}{X(x)} .$$

This implies that there exists a constant λ such that

$$\frac{1}{D}\frac{T'(t)}{T(t)} = \frac{X''(x)}{X(x)} = \lambda , \tag{2.1.16}$$

From Equation (2.1.16), we obtained the following ODEs,

$$T'(t) - \lambda DT(t) = 0 \tag{2.1.17}$$
$$X''(x) - \lambda X(x) = 0 , \tag{2.1.18}$$

and from the boundary conditions in Equation (2.1.15), we have the following boundary conditions

$$X'(-L) = 0 \quad \text{and} \quad X'(L) = 0 , \tag{2.1.19}$$

Now, we can solve the second order ODE in Equation (2.1.18) together with the boundary conditions in Equation (2.1.19). For this equation, we must have $\lambda < 0$ for a non-trivial solution. Let $\lambda = -\alpha^2$, then the general solution of Equation (2.1.18) is

$$X(x) = A\cos\alpha x + B\sin\alpha x , \qquad (A \text{ and } B \text{ are constants}) .$$

Applying the boundary conditions in Equation (2.1.19), we have $B = 0$ and

$$\alpha_n = \frac{n\pi}{L} , \qquad n \geq 1 .$$

Since $\lambda = -\alpha^2$, we have infinitely many value of λ

$$\lambda_n = -\left(\frac{n\pi}{L}\right)^2 , \qquad n \geq 1 ,$$

and thus, we have an infinite set of solutions

$$X_n(x) = A_n \cos\left(\frac{n\pi}{L}x\right) , \qquad n \geq 1 .$$

Substituting the value of λ into Equation (2.1.17), we have

$$T_n'(t) + D\left(\frac{n\pi}{L}\right)^2 T_n(t) = 0 , \qquad n \geq 1$$

and the solutions are

$$T_n(t) = C_n e^{-D\left(\frac{n\pi}{L}\right)^2 t} , \qquad n \geq 1 \qquad (C_n \text{ are constants}) . \tag{2.1.20}$$

Recall, $f(x,t) = X(x)T(t)$, therefore, $f_n(x,t) = X_n(x)T_n(t)$. Thus,

$$f_n(x,t) = A_n C_n \cos\left(\frac{n\pi}{L}x\right) e^{-D\left(\frac{n\pi}{L}\right)^2 t}$$
$$f_n(x,t) = a_n \cos\left(\frac{n\pi}{L}x\right) e^{-D\left(\frac{n\pi}{L}\right)^2 t}\ , \qquad (A_n C_n = a_n)\ .$$

Using the principle of superposition, we have

$$f(x,t) = \frac{a_0}{2} + \sum_{n\geq 1} a_n \cos\left(\frac{n\pi}{L}x\right) e^{-D\left(\frac{n\pi}{L}\right)^2 t}\ . \tag{2.1.21}$$

Here, our initial condition is

$$f(x,0) = \phi(x) = \begin{cases} 0, & -a \leq x \leq a \\ 1, & \text{otherwise.} \end{cases} \tag{2.1.22}$$

Applying this initial condition, we have

$$\frac{a_0}{2} + \sum_{n\geq 1} a_n \cos\left(\frac{n\pi}{L}x\right) = \phi(x)\ . \tag{2.1.23}$$

To get a_0, we integrate each term of this equation over the interval $[-L, L]$,

$$\int_{-L}^{L} \frac{a_0}{2}\ \mathrm{d}x + \sum_{n\geq 1} a_n \int_{-L}^{L} \cos\left(\frac{n\pi}{L}x\right)\ \mathrm{d}x = \int_{-L}^{L} \phi(x)\ \mathrm{d}x\ ,$$

from this equation, we have

$$a_0 = \frac{1}{L}\int_{-L}^{L} \phi(x)\ \mathrm{d}x\,.$$

Implementing the step function in the initial condition in Equation (2.1.22) gives

$$a_0 = 2\left(1 - \frac{a}{L}\right)\ . \tag{2.1.24}$$

Similarly, to get a_n, we multiply each term of Equation (2.1.23) by $\cos\left(\frac{n\pi}{L}x\right)$ and then integrate over $[-L, L]$

$$\frac{a_0}{2}\int_{-L}^{L} \cos\left(\frac{n\pi}{L}x\right)\ \mathrm{d}x + \sum_{n\geq 1} a_n \int_{-L}^{L} \cos\left(\frac{n\pi}{L}x\right)\cos\left(\frac{n\pi}{L}x\right)\ \mathrm{d}x = \int_{-L}^{L} \phi(x)\cos\left(\frac{n\pi}{L}x\right)\ \mathrm{d}x\,.$$

Since

$$\int_{-L}^{L} \cos^2\left(\frac{n\pi}{L}x\right)\ \mathrm{d}x = L \quad \text{and} \quad \int_{-L}^{L} \cos\left(\frac{n\pi}{L}x\right)\ \mathrm{d}x = 0,$$

we have

$$a_n = \frac{1}{L}\int_{-L}^{L} \phi(x)\cos\left(\frac{n\pi}{L}x\right)\ \mathrm{d}x\ .$$

Also, implementing the step function in the initial condition in Equation (2.1.22) gives

$$a_n = -\frac{2}{n\pi}\sin\left(\frac{n\pi a}{L}x\right) \ . \tag{2.1.25}$$

Therefore,

$$f(x,t) = \left(1-\frac{a}{L}\right) - \sum_{n\geq 1}\left(\frac{2}{n\pi}\sin\left(\frac{n\pi a}{L}\right)\right)\ \cos\left(\frac{n\pi}{L}x\right) e^{-D\left(\frac{n\pi}{L}\right)^2 t}\,. \tag{2.1.26}$$

Next, we integrate the function $f(x,t)$ as defined in Equation (2.1.26) over the entire bleached region,

$$H(t,D) = \int_{-a}^{a}\left(1-\frac{a}{L}\right)\ \mathrm{d}x - \int_{-a}^{a}\sum_{n\geq 1}\left(\frac{2}{n\pi}\sin\left(\frac{n\pi a}{L}\right)\right) e^{-D\left(\frac{n\pi}{L}\right)^2 t}\ \cos\left(\frac{n\pi}{L}x\right)\ \mathrm{d}x\ ,$$

evaluating the integral and simplifying, we have

$$H(t,D) = 2a\left(1-\frac{a}{L}\right) - \sum_{n\geq 1}\frac{4L}{n^2\pi^2}\ \sin^2\left(\frac{n\pi a}{L}\right) e^{-D\left(\frac{n\pi}{L}\right)^2 t}\ .$$

Since the length of the cell $L_c = 2L$ and the width of the bleached region $w_b = 2a$, then we can write this equations as

$$H(t,D) = w_b\left(1-\frac{w_b}{L_c}\right) - \frac{2L_c}{\pi^2}\sum_{n\geq 1}\frac{1}{n^2}\ \sin^2\left(\frac{n\pi\, w_b}{L_c}\right) e^{-D\left(\frac{2n\pi}{L_c}\right)^2 t}\ . \tag{2.1.27}$$

This is the model for the Fourier Series approach.

2.2 Derivation of the two-dimensional models

For the two-dimensional models, we considered the disc bleach spot (Figure 2.2) and the square bleach spot (Figure 2.3). These models can be used to model the mobility of protein in a cell membrane.

2.2.1 Disk bleach spot. In developing a model for this bleach spot, we consider the diffusion equation in the cylindrical coordinate given as

$$\frac{1}{r}\frac{\partial V}{\partial r} + \frac{\partial^2 V}{\partial r^2} + \frac{1}{r^2}\frac{\partial^2 V}{\partial \theta^2} = \frac{1}{D}\frac{\partial V}{\partial t}\ , \tag{2.2.1}$$

where $V(r,\theta,t)$ is the fluorescence intensity on the disc at time t and $0 \leq r \leq a$ is the radius of the disc.

With the boundary conditions,

$$|V(0,\theta,t)| < \infty\ , \quad V(r,0,t) = V(r,2\pi,t)\ ,\ \text{and}\quad V_\theta(r,0,t) = V_\theta(r,2\pi,t)\ , \quad 0 \leq r \leq a \tag{2.2.2}$$

$$V(a,\theta,t) = 1\ , \quad 0 \leq \theta \leq 2\pi \quad \text{and} \quad t \geq 0\ . \tag{2.2.3}$$

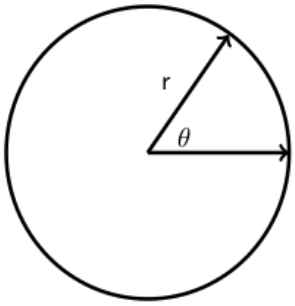

Figure 2.2: A disc bleach spot.

We assumed that the initial fluorescent intensity everywhere on the cell surface is unity except in the interior part of the disc where it is zero as a result of bleaching, i.e

$$V(r,\theta,0) = \phi(r,\theta) = 0 \ , \quad 0 \le r < a \tag{2.2.4}$$

and that the intensity at the edge of the disc is unity at all time (this is satisfied by the boundary condition in Equation (2.2.3)).

We begin by partitioning the desired solution into two solutions as shown below,

$$V(r,\theta,t) = w(r,\theta) + u(r,\theta,t) \tag{2.2.5}$$

where $w(r,\theta)$ is the steady-state solution and $u(r,\theta,t)$ is the time-dependent solution.

In our case, we make the steady-state solution to be a constant ($w(r,\theta) = 1$), therefore,

$$V(r,\theta,t) = 1 + u(r,\theta,t) \ . \tag{2.2.6}$$

Substituting $V(r,\theta,t)$ as defined in Equation (2.2.6) into Equation (2.2.1), we have

$$\frac{1}{r}\frac{\partial u}{\partial r} + \frac{\partial^2 u}{\partial r^2} + \frac{1}{r^2}\frac{\partial^2 u}{\partial \theta^2} = \frac{1}{D}\frac{\partial u}{\partial t} \ . \tag{2.2.7}$$

This equation satisfies the boundary conditions,

$$|u(0,\theta,t)| < \infty \ , \quad u(r,0,t) = u(r,2\pi,t) \ , \text{ and } \quad u_\theta(r,0,t) = u_\theta(r,2\pi,t) \ , \quad 0 \le r \le a \ , \tag{2.2.8}$$

$$u(a,\theta,t) = 0 \ , \quad 0 \le \theta \le 2\pi \ , \ t \ge 0 \ . \tag{2.2.9}$$

Now, we can solve Equation (2.2.7) together with the boundary conditions in Equations (2.2.8) and (2.2.9). Using the method of separation of variables, let

$$u(r,\theta,t) = R(r)\Theta(\theta)T(t) \ ,$$

then Equation (2.2.7) becomes,

$$\frac{1}{r}R'(r)\Theta(\theta)T(t) + R''(r)\Theta(\theta)T(t) + \frac{1}{r^2}R(r)\Theta''(\theta)T(t) = \frac{1}{D}R(r)\Theta(\theta)T'(t) \ .$$

We divide each term of this equation by $R(r)\Theta(\theta)T(t)$, to obtain

$$\frac{1}{r}\frac{R'(r)}{R(r)} + \frac{R''(r)}{R(r)} + \frac{1}{r^2}\frac{\Theta''(\theta)}{\Theta(\theta)} = \frac{1}{D}\frac{T'(t)}{T(t)} ,$$

and this implies that there exists a constant $-\alpha^2$ such that

$$\frac{1}{r}\frac{R'(r)}{R(r)} + \frac{R''(r)}{R(r)} + \frac{1}{r^2}\frac{\Theta''(\theta)}{\Theta(\theta)} = \frac{1}{D}\frac{T'(t)}{T(t)} = -\alpha^2 .$$

From this equation, we have

$$\frac{1}{D}\frac{T'(t)}{T(t)} = -\alpha^2$$
$$T'(t)+\alpha^2 DT(t) = 0$$

and

$$\frac{1}{r}\frac{R'(r)}{R(r)} + \frac{R''(r)}{R(r)} + \frac{1}{r^2}\frac{\Theta''(\theta)}{\Theta(\theta)} = -\alpha^2$$
$$\frac{\frac{1}{r}R'(r)\Theta(\theta) + R''(r)\Theta(\theta) + \frac{1}{r^2}R(r)\Theta''(\theta)}{R(r)\Theta(\theta)} = -\alpha^2 .$$

Multiply both sides of this equation by r^2 to get

$$\frac{rR'(r) + r^2R''(r) + r^2\alpha^2R(r)}{R(r)} = -\frac{\Theta''(\theta)}{\Theta(\theta)} .$$

This also implies that there exists another constant β^2 such that

$$\frac{rR'(r) + r^2R''(r) + r^2\alpha^2R(r)}{R(r)} = -\frac{\Theta''(\theta)}{\Theta(\theta)} = \beta^2 , \tag{2.2.10}$$

Form Equation (2.2.10), we have

$$\frac{rR'(r) + r^2R''(r) + r^2\alpha^2R(r)}{R(r)} = \beta^2 .$$

Simplifying this equation, we obtain

$$r^2R''(r) + rR'(r) + (r^2\alpha^2 - \beta^2)R(r) = 0 .$$

Also, form Equation (2.2.10), we have

$$-\frac{\Theta''(\theta)}{\Theta(\theta)} = \beta^2$$
$$\Theta''(\theta) + \beta^2\Theta(\theta) = 0$$

Therefore, the PDE in Equation (2.2.7) has been transform into the following ODEs

$$T'(t)+\alpha^2 DT(t) = 0 \ , \tag{2.2.11}$$
$$r^2R''(r) + rR'(r)+(r^2\alpha^2 - \beta^2)R(r) = 0 \ , \tag{2.2.12}$$
$$\Theta''(\theta)+\beta^2\Theta(\theta) = 0 \ . \tag{2.2.13}$$

From the boundary conditions in Equation (2.2.8), we have

$$\begin{aligned} u(r,0,t) = u(r,2\pi,t) \quad &\Longrightarrow \quad R(r)\,\Theta(0)\,T(t) = R(r)\,\Theta(2\pi)\,T(t) \quad \Longrightarrow \quad \Theta(0) = \Theta(2\pi) \\ u_\theta(r,0,t) = u_\theta(r,2\pi,t) \quad &\Longrightarrow \quad R(r)\,\Theta'(0)\,T(t) = R(r)\,\Theta'(2\pi)\,T(t) \quad \Longrightarrow \quad \Theta'(0) = \Theta'(2\pi) \ . \end{aligned}$$

Solving the second order ODE in Equation (2.2.13), we obtain the general solution

$$\Theta(\theta) = A\cos\theta\beta + B\sin\theta\beta \ , \qquad (A \text{ and } B \text{ are constants}) \ .$$

Applying the boundary conditions

$$\Theta(0) = \Theta(2\pi) \quad \text{and} \quad \Theta'(0) = \Theta'(2\pi) \ ,$$

we have

$$A = A\cos 2\pi\beta \quad \text{and} \quad B = B\cos 2\pi\beta \ .$$

For these equations to hold, β must be an integer, therefore, $\beta = n$, $n = 0, 1, 2, \ldots$. Thus, the solution of the boundary value problem is

$$\Theta_n(\theta) = A_n\cos n\theta + B_n\sin n\theta \ , \qquad n = 0, 1, 2, \ldots$$

Now, let us consider Equation (2.2.12)

$$r^2R''(r) + rR'(r)+(r^2\alpha^2 - \beta^2)R(r) = 0 \ .$$

Since $\beta = n$, we have

$$r^2R_n''(r) + rR_n'(r)+(r^2\alpha^2 - n^2)R_n(r) = 0 \ , \qquad n = 0, 1, 2, \ldots \tag{2.2.14}$$

We can use the method of Frobenius to obtain the general solution

$$R_n(r) = C_n\ J_n(\alpha r) + E_n\ Y_n(\alpha r) \tag{2.2.15}$$

where C_n and E_n are constants,

$$J_n(\alpha r) = \sum_{k=0}^{\infty} \frac{(-1)^k}{k!\ \Gamma(k+n+1)} \left(\frac{\alpha r}{2}\right)^{2k+n} \quad \text{and} \quad J_{-n}(\alpha r) = \sum_{k=0}^{\infty} \frac{(-1)^k}{k!\ \Gamma(k-n+1)} \left(\frac{\alpha r}{2}\right)^{2k-n}$$

are Bessel functions of the first kind of order n and order $-n$ respectively.

$$Y_n(\alpha r) = \frac{\cos(n\pi)J_n(\alpha r) - J_{-n}(\alpha r)}{\sin(n\pi)} \ , \qquad \alpha r > 0$$

is a Bessel function of the second kind of order n.

From the boundary conditions $|u(0,\theta,t)| < \infty$ and $u(a,\theta,t) = 0$, we derived $|R(0)| < \infty$ and $R(a) = 0$. We need to apply these boundary conditions to the solution in Equation (2.2.15).

For $|R(0)| < \infty$, we know that $|J_n(\alpha r)| \leq 1$ for $n = 0, 1, 2, \ldots$. But as $r \longrightarrow 0$, $Y_n(\alpha r) \longrightarrow -\infty$. Therefore, for the condition $|R(0)| < \infty$ to hold, E_n must be zero and so, $R_n(r) = C_n\ J_n(\alpha r)$. For $R(a) = 0$,

$$R_n(a) = C_n J_n(\alpha a) = 0$$
$$C_n \neq 0, \quad \therefore \quad J_n(\alpha a) = 0\ .$$

Since the Bessel function behaves in a sinusoidal way, $J_n(\alpha a) = 0$ for infinitely many α for each n. That is

$$J_n(\alpha_{ni} a) = 0 \qquad \text{for} \qquad i = 1, 2, \ldots$$

where α_{ni} is the i^{th} zero of the Bessel function of order n.

$$R_{ni}(r) = C_{ni}\ J_n(\alpha_{ni} r) \qquad n = 0, 1, 2, \ldots\ , \quad i = 1, 2, \ldots$$

From Equation (2.2.11), we have

$$T'_{ni}(t) + \alpha_{ni} D T_{ni}(t) = 0\ .$$

Solving this equation, we obtain

$$T_{ni}(t) = G_{ni} e^{-\alpha_{ni}^2 Dt} \qquad (G_{ni}, \text{constant}).$$

Recall, $u(r,\theta,t) = R(r)\Theta(\theta)T(T)$, therefore, $u_{ni}(r,\theta,t) = R_{ni}(r)\Theta_n(\theta)T_{ni}(T)$. Thus,

$$u_{ni}(r,\theta,t) = C_{ni} J_n(\alpha_{ni} r)(A_n \cos n\theta + B_n \sin n\theta) G_{ni} e^{-\alpha_{ni}^2 Dt}. \tag{2.2.16}$$

Using the principle of superposition, we have

$$u(r,\theta,t) = \sum_{n=0}^{\infty}\sum_{i=0}^{\infty} C_{ni} J_n(\alpha_{ni} r)(A_n \cos n\theta + B_n \sin n\theta) G_{ni} e^{-\alpha_{ni}^2 Dt}$$
$$u(r,\theta,t) = \sum_{n=0}^{\infty}\sum_{i=0}^{\infty} J_n(\alpha_{ni} r)(a_{ni} \cos n\theta + b_{ni} \sin n\theta) e^{-\alpha_{ni}^2 Dt} \qquad (a_{ni} = C_{ni}A_n,\ \ b_{ni} = C_{ni}B_n)\ .$$

We recall from Equation (2.2.6) that

$$V(r,\theta,t) = 1 + u(r,\theta,t)\ .$$

Therefore,

$$V(r,\theta,t) = 1 + \sum_{n=0}^{\infty}\sum_{i=0}^{\infty} J_n(\alpha_{ni} r)(a_{ni} \cos n\theta + b_{ni} \sin n\theta) e^{-\alpha_{ni}^2 Dt}. \tag{2.2.17}$$

We assumed that the distribution of fluorescence intensity on the disc is symmetric and does not depend on the angle θ, therefore, the solution of Equation (2.2.1) becomes:

$$V(r,t) = 1 + \sum_{i=0}^{\infty} d_i \; J_0(\alpha_i r) e^{-\alpha_i^2 Dt} \qquad (d_i, \text{ constant}) \tag{2.2.18}$$

and the initial condition in Equation (2.2.4) becomes

$$V(r,0) = \phi(r) = 0 \; , \quad 0 \leq r < a \tag{2.2.19}$$

Now, let us apply the initial condition in Equation (2.2.19) to the solution in Equation (2.2.18). Applying this conditions, we have

$$1 + \sum_{i=0}^{\infty} d_i \; J_0(\alpha_i r) \; = 0 \; .$$

If we then multiply both sides of this result by $rJ_0(\alpha_i r)$ and integrate from 0 to a,

$$\int_0^a r \; J_0(\alpha_i r) d_i \; J_0(\alpha_i r) \;\; \mathsf{d}r = -\int_0^a r \; J_0(\alpha_i r) \mathsf{d}r$$

$$d_i = \frac{-\int_0^a r \; J_0(\alpha_i r) \mathsf{d}r}{\int_0^a r \; \left[J_0(\alpha_i r)\right]^2 \mathsf{d}r} = \frac{-2}{a \; \alpha_i \; J_1(\alpha_i \; a)} \; .$$

Therefore,

$$V(r,t) = 1 - \sum_{i=0}^{\infty} \left(\frac{2}{a \; \alpha_i \; J_1(\alpha_i \; a)} \right) \; J_0(\alpha_i r) \; e^{-\alpha_i^2 Dt} \; .$$

Next, we integrate the function $V(r,t)$ over the entire bleached region (the disc),

$$\begin{aligned} H(t,D) &= \int_0^a 2\pi r \; \mathsf{d}r - \int_0^a \sum_{i=0}^{\infty} 2\pi r \left(\frac{2}{a \; \alpha_i \; J_1(\alpha_i \; a)} \right) \; J_0(\alpha_i r) \; e^{-\alpha_i^2 Dt} \; \mathsf{d}r \\ &= 2\pi \int_0^a r \; \mathsf{d}r - \sum_{i=0}^{\infty} \left(\frac{4\pi}{a \; \alpha_i \; J_1(\alpha_i \; a)} \right) \; e^{-\alpha_i^2 Dt} \int_0^a r J_0(\alpha_i r) \; \mathsf{d}r \\ &= 2\pi \left[\frac{r^2}{2} \right]_0^a - \sum_{i=0}^{\infty} \frac{4\pi e^{-\alpha_i^2 Dt}}{a \; \alpha_i \; J_1(\alpha_i \; a)} \; \left(\frac{a J_1(\alpha_i \; a)}{\alpha_i} \right) \; . \end{aligned}$$

Simplifying this equation, we get

$$H(t,D) = a^2\pi - \sum_{i=0}^{\infty} \frac{4\pi}{\alpha_i^2} \; e^{-\alpha_i^2 Dt}$$

where a is the radius of the disc and α_i is the i^{th} zero of the Bessel function of the first kind of order zero.

This function can be used to model the FRAP experiment with a disc bleach spot.

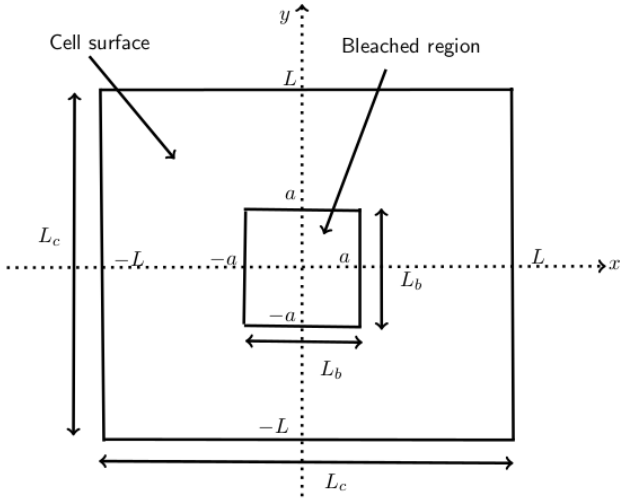

Figure 2.3: A square bleach spot.

2.2.2 Square bleach spot. In deriving the model for the square bleach spot, we used the two-dimensional diffusion equation in xy coordinates given by

$$\frac{1}{D}\frac{\partial u}{\partial t} = \frac{\partial^2 u}{\partial x^2} + \frac{\partial^2 u}{\partial y^2} \tag{2.2.20}$$

where $u(x, y, t)$ is the fluorescence intensity at position (x, y) and time t, and D is the diffusion coefficient.

We assumed the surface of the cell is a square with sides $L_c = 2L$ ($[-L, L] \times [-L, L]$) and the bleached region is a smaller square on the surface of the cell with sides $L_b = 2a$ ($[-a, a] \times [-a, a]$). We also assumed the boundaries of the cell satisfies the Neumann boundary conditions,

$$\begin{aligned} u_x(-L, y, t) &= u_x(L, y, t) = 0 \\ u_y(x, -L, t) &= u_y(x, L, t) = 0 \ , \end{aligned} \tag{2.2.21}$$

and that the initial fluorescence intensity on the cell surface is unity everywhere except in the bleached region where the intensity is zero. This can be written as

$$u(x, y, 0) = \phi(x, y) = \begin{cases} 0, & -a \le x \le a \, , \ -a \le y \le a \\ 1, & \text{otherwise.} \end{cases} \tag{2.2.22}$$

We begin by using the method of separation of variables. Let

$$u(x, y, t) = X(x)Y(y)T(t) \ ,$$

then Equation (2.2.20) becomes

$$\frac{1}{D}X(x)Y(y)T'(t) = X''(x)Y(y)T(t) + X(x)Y''(y)T(t) \ .$$

Dividing each term of this equation by $X(x)Y(y)T(t)$, we obtain

$$\frac{1}{D}\frac{T'(t)}{T(t)} = \frac{X''(x)}{X(x)} + \frac{Y''(y)}{Y(y)} \ .$$

Let

$$\frac{1}{D}\frac{T'(t)}{T(t)} = \frac{X''(x)}{X(x)} + \frac{Y''(y)}{Y(y)} = -(\alpha^2 + \beta^2) \ . \tag{2.2.23}$$

From this equation, we have

$$\frac{1}{D}\frac{T'(t)}{T(t)} = -(\alpha^2 + \beta^2) \ ,$$
$$T'(t) + (\alpha^2 + \beta^2)DT(t) = 0 \ .$$

Also, from Equation (2.2.23),

$$\frac{X''(x)}{X(x)} + \frac{Y''(y)}{Y(y)} = -(\alpha^2 + \beta^2)$$
$$\frac{X''(x)}{X(x)} + \alpha^2 = -\left(\frac{Y''(y)}{Y(y)} + \beta^2\right) \ .$$

For this equation to hold, both sides of the equation must be equal to zero. That is,

$$\frac{X''(x)}{X(x)} + \alpha^2 = 0 \qquad \text{and} \qquad \frac{Y''(y)}{Y(y)} + \beta^2 = 0$$
$$X''(x) + \alpha^2 X(x) = 0 \qquad Y''(y) + \beta^2 Y(y) = 0 \ .$$

We have transformed the PDE in Equation (2.2.20) into the following ODEs

$$T'(t) + (\alpha^2 + \beta^2)DT(t) = 0 \tag{2.2.24}$$
$$X''(x) + \alpha^2 X(x) = 0 \tag{2.2.25}$$
$$Y''(y) + \beta^2 Y(y) = 0 \ . \tag{2.2.26}$$

From the boundary conditions in Equation (2.2.21), we have

$$X'(-L) = X'(L) = 0 \tag{2.2.27}$$
$$Y'(-L) = Y'(L) = 0 \ . \tag{2.2.28}$$

Now, let us consider the ODE in Equation (2.2.25). The general solution of this equation is

$$X(x) = A\cos\alpha x + B\sin\alpha x \ , \qquad (A \text{ and } B \text{ are constants})$$

Applying the boundary conditions in Equation (2.2.27) to this solution, we have

$$B = 0 \quad \text{and} \quad \alpha_n = \frac{n\pi}{L} \ , \qquad n \geq 1$$
$$\therefore \quad X_n(x) = A_n \cos\left(\frac{n\pi}{L}x\right) \ , \qquad n \geq 1 \ . \tag{2.2.29}$$

Similarly, the general solution of Equation (2.2.26) is

$$Y(y) = C\cos\beta y + G\sin\beta y \ , \qquad (C \text{ and } G \text{ are constants})$$

and applying the boundary conditions in Equation (2.2.28), we have

$$G = 0 \quad \text{and} \quad \beta_m = \frac{m\pi}{L} \ , \qquad m \geq 1$$
$$\therefore \quad Y_m(x) = C_m \cos\left(\frac{m\pi}{L}y\right) \ , \qquad m \geq 1 \ . \tag{2.2.30}$$

Substituting $\alpha_n = \frac{n\pi}{L}$ and $\beta_m = \frac{m\pi}{L}$ into Equation (2.2.24), we obtain

$$T'_{n,m}(t) + D\left(\left(\frac{n\pi}{L}\right)^2 + \left(\frac{m\pi}{L}\right)^2\right) T_{n,m}(t) = 0\ , \qquad n, m \geq 1$$

and the solution of this equation is

$$T_{n,m}(t) = E_{n,m} e^{-D\frac{\pi^2}{L^2}(n^2+m^2)t}\ , \qquad n, m \geq 1. \tag{2.2.31}$$

Recall that $u(x,y,t) = X(x)Y(y)T(t)$, therefore, $u_{n,m}(x,y,t) = X_n(x)Y_m(y)T_{n,m}(t)$. Substituting the results in Equations (2.2.29), (2.2.30) and (2.2.31) into this equation,

$$u_{n,m}(x,y,t) = A_n \cos\left(\frac{n\pi}{L}x\right) C_m \cos\left(\frac{m\pi}{L}y\right) E_{n,m} e^{-D\frac{\pi^2}{L^2}(n^2+m^2)t}\ .$$

Using the principle of superposition,

$$\begin{aligned} u(x,y,t) &= u_{0,0}(x,y,t) + \sum_{n\geq 1} u_{n,0}(x,y,t) + \sum_{m\geq 1} u_{0,m}(x,y,t) + \sum_{n\geq 1}\sum_{m\geq 1} u_{n,m}(x,y,t) \\ u(x,y,t) &= a_{0,0} + \sum_{n\geq 1} a_{n,0} \cos\left(\frac{n\pi}{L}x\right) e^{-D\frac{\pi^2}{L^2}n^2 t} + \sum_{m\geq 1} a_{0,m} \cos\left(\frac{m\pi}{L}y\right) e^{-D\frac{\pi^2}{L^2}m^2 t} \\ &\quad + \sum_{n\geq 1}\sum_{m\geq 1} A_n \cos\left(\frac{n\pi}{L}x\right) C_m \cos\left(\frac{m\pi}{L}y\right) E_{n,m} e^{-D\frac{\pi^2}{L^2}(n^2+m^2)t}\ . \end{aligned}$$

Therefore, the general solution of the PDE in Equation (2.2.20) is

$$\begin{aligned} u(x,y,t) &= a_{0,0} + \sum_{n\geq 1} a_{n,0} \cos\left(\frac{n\pi}{L}x\right) e^{-D\frac{\pi^2}{L^2}n^2 t} + \sum_{m\geq 1} a_{0,m} \cos\left(\frac{m\pi}{L}y\right) e^{-D\frac{\pi^2}{L^2}m^2 t} \\ &\quad + \sum_{n\geq 1}\sum_{m\geq 1} a_{n,m} \cos\left(\frac{n\pi}{L}x\right) \cos\left(\frac{m\pi}{L}y\right) e^{-D\frac{\pi^2}{L^2}(n^2+m^2)t}\ , \qquad (A_n C_m E_{n,m} = a_{n,m}) \end{aligned} \tag{2.2.32}$$

Next, we apply the initial condition in Equation (2.2.22). This initial condition can be written in the form

$$u(x,y,0) = \phi(x,y) = \begin{cases} 1, & -L \leq x < -a\ ,\ -L \leq y \leq L \\ 1, & -a \leq x \leq a\ ,\ -L \leq y < -a \\ 0, & -a \leq x \leq a\ ,\ -a \leq y \leq a \\ 1, & a < x \leq L\ ,\ -L \leq y \leq L \\ 1, & -a \leq x \leq a\ ,\ a < y \leq L \end{cases} \tag{2.2.33}$$

First, we apply the initial condition as function of $\phi(x,y)$,

$$\begin{aligned} u(x,y,0) &= a_{0,0} + \sum_{n\geq 1} a_{n,0} \cos\left(\frac{n\pi}{L}x\right) + \sum_{m\geq 1} a_{0,m} \cos\left(\frac{m\pi}{L}y\right) \\ &\quad + \sum_{n\geq 1}\sum_{m\geq 1} a_{n,m} \cos\left(\frac{n\pi}{L}x\right) \cos\left(\frac{m\pi}{L}y\right) = \phi(x,y)\ . \end{aligned} \tag{2.2.34}$$

To get a_{00}, we integrate each term of the equation over the square $([-L,L]\times[-L,L])$

$$\int_{-L}^{L}\int_{-L}^{L} a_{0,0}\,\mathrm{d}x\,\mathrm{d}y+\sum_{n\geq 1} a_{n,0}\int_{-L}^{L}\int_{-L}^{L}\cos\left(\frac{n\pi}{L}x\right)\,\mathrm{d}x\,\mathrm{d}y$$
$$+\sum_{m\geq 1} a_{0,m}\int_{-L}^{L}\int_{-L}^{L}\cos\left(\frac{m\pi}{L}y\right)\,\mathrm{d}x\,\mathrm{d}y$$
$$+\sum_{n\geq 1}\sum_{m\geq 1} a_{n,m}\int_{-L}^{L}\int_{-L}^{L}\cos\left(\frac{n\pi}{L}x\right)\cos\left(\frac{m\pi}{L}y\right)\,\mathrm{d}x\,\mathrm{d}y=\int_{-L}^{L}\int_{-L}^{L}\phi(x,y)\,\mathrm{d}x\,\mathrm{d}y\ . \quad (2.2.35)$$

Since

$$\int_{-L}^{L}\cos\left(\frac{n\pi}{L}x\right)\,\mathrm{d}x=0\quad\text{and}\quad\int_{-L}^{L}\cos\left(\frac{n\pi}{L}y\right)\,\mathrm{d}y=0\ , \quad (2.2.36)$$

Equation (2.2.35), reduces to

$$\int_{-L}^{L}\int_{-L}^{L} a_{0,0}\,\mathrm{d}x\,\mathrm{d}y=\int_{-L}^{L}\int_{-L}^{L}\phi(x,y)\,\mathrm{d}x\,\mathrm{d}y$$
$$a_{0,0}=\frac{1}{4L^2}\int_{-L}^{L}\int_{-L}^{L}\phi(x,y)\,\mathrm{d}x\,\mathrm{d}y\ .$$

Implementing the step function in the initial condition in Equation (2.2.33), we have

$$a_{0,0}=\frac{1}{4L^2}\left[\int_{-L}^{-a}\int_{-L}^{L}1\,\mathrm{d}x\,\mathrm{d}y+\int_{-a}^{a}\int_{-L}^{-a}1\,\mathrm{d}x\,\mathrm{d}y+\int_{-a}^{a}\int_{-a}^{a}0\,\mathrm{d}x\,\mathrm{d}y\right.$$
$$\left.+\int_{a}^{L}\int_{-L}^{L}\mathrm{d}x\,\mathrm{d}y+\int_{-a}^{a}\int_{a}^{L}1\,\mathrm{d}x\,\mathrm{d}y\right]$$
$$a_{0,0}=1-\frac{a^2}{L^2}\ .$$

To get $a_{n,0}$, we multiply each term of Equation (2.2.34) by $\cos\left(\frac{n\pi}{L}x\right)$ and then integrate over the square $([-L,L]\times[-L,L])$,

$$\int_{-L}^{L}\int_{-L}^{L} a_{0,0}\cos\left(\frac{n\pi}{L}x\right)\,\mathrm{d}x\,\mathrm{d}y+\sum_{n\geq 1} a_{n,0}\int_{-L}^{L}\int_{-L}^{L}\cos^2\left(\frac{n\pi}{L}x\right)\,\mathrm{d}x\,\mathrm{d}y$$
$$+\sum_{m\geq 1} a_{0,m}\int_{-L}^{L}\int_{-L}^{L}\cos\left(\frac{n\pi}{L}x\right)\cos\left(\frac{m\pi}{L}y\right)\,\mathrm{d}x\,\mathrm{d}y$$
$$+\sum_{n\geq 1}\sum_{m\geq 1} a_{n,m}\int_{-L}^{L}\int_{-L}^{L}\cos^2\left(\frac{n\pi}{L}x\right)\cos\left(\frac{m\pi}{L}y\right)\,\mathrm{d}x\,\mathrm{d}y$$
$$=\int_{-L}^{L}\int_{-L}^{L}\phi(x,y)\cos\left(\frac{n\pi}{L}x\right)\,\mathrm{d}x\,\mathrm{d}y\ . \quad (2.2.37)$$

Based on the results in Equation (2.2.36), Equation (2.2.37) reduces to

$$a_{n,0}\int_{-L}^{L}\int_{-L}^{L}\cos^2\left(\frac{n\pi}{L}x\right)\,\mathrm{d}x\,\mathrm{d}y=\int_{-L}^{L}\int_{-L}^{L}\phi(x,y)\cos\left(\frac{n\pi}{L}x\right)\,\mathrm{d}x\,\mathrm{d}y$$
$$a_{n,0}=\frac{1}{2L^2}\int_{-L}^{L}\int_{-L}^{L}\phi(x,y)\cos\left(\frac{n\pi}{L}x\right)\,\mathrm{d}x\,\mathrm{d}y\ .$$

Implementing the step function in the initial condition in Equation (2.2.33), we have

$$\begin{aligned} a_{n,0} &= \frac{1}{2L^2}\left[\int_{-L}^{-a}\int_{-L}^{L}\cos\left(\frac{n\pi}{L}x\right)\,\mathrm{d}x\,\mathrm{d}y+\int_{-a}^{a}\int_{-L}^{-a}\cos\left(\frac{n\pi}{L}x\right)\,\mathrm{d}x\,\mathrm{d}y\right.\\ &\quad\left.+\int_{-a}^{a}\int_{-a}^{a}0\,\mathrm{d}x\,\mathrm{d}y+\int_{a}^{L}\int_{-L}^{L}\cos\left(\frac{n\pi}{L}x\right)\,\mathrm{d}x\,\mathrm{d}y+\int_{-a}^{a}\int_{a}^{L}\cos\left(\frac{n\pi}{L}x\right)\,\mathrm{d}x\,\mathrm{d}y\right]\\ a_{n,0} &= -\frac{2a}{n\pi L}\sin\left(\frac{n\pi}{L}a\right)\ . \end{aligned}$$

Similarly, to get $a_{0,m}$, we multiply each term of Equation (2.2.34) by $\cos\left(\frac{m\pi}{L}y\right)$ and then integrate over the square $([-L,L]\times[-L,L])$,

$$\begin{aligned} &\int_{-L}^{L}\int_{-L}^{L}a_{0,0}\cos\left(\frac{m\pi}{L}y\right)\,\mathrm{d}x\,\mathrm{d}y+\sum_{n\geq 1}a_{n,0}\int_{-L}^{L}\int_{-L}^{L}\cos\left(\frac{m\pi}{L}y\right)\cos\left(\frac{n\pi}{L}x\right)\,\mathrm{d}x\,\mathrm{d}y\\ &+\sum_{m\geq 1}a_{0,m}\int_{-L}^{L}\int_{-L}^{L}\cos^2\left(\frac{m\pi}{L}y\right)\,\mathrm{d}x\,\mathrm{d}y+\sum_{n\geq 1}\sum_{m\geq 1}a_{n,m}\int_{-L}^{L}\int_{-L}^{L}\cos\left(\frac{n\pi}{L}x\right)\cos^2\left(\frac{m\pi}{L}y\right)\,\mathrm{d}x\,\mathrm{d}y\\ &\quad=\int_{-L}^{L}\int_{-L}^{L}\phi(x,y)\cos\left(\frac{m\pi}{L}y\right)\,\mathrm{d}x\,\mathrm{d}y\ . \end{aligned}\tag{2.2.38}$$

Using the results in Equation (2.2.36), Equation (2.2.38) reduces to

$$\begin{aligned} a_{0,m}\int_{-L}^{L}\int_{-L}^{L}\cos^2\left(\frac{m\pi}{L}y\right)\,\mathrm{d}x\,\mathrm{d}y &= \int_{-L}^{L}\int_{-L}^{L}\phi(x,y)\cos\left(\frac{m\pi}{L}y\right)\,\mathrm{d}x\,\mathrm{d}y\\ a_{0,m} &= \frac{1}{2L^2}\int_{-L}^{L}\int_{-L}^{L}\phi(x,y)\cos\left(\frac{m\pi}{L}y\right)\,\mathrm{d}x\,\mathrm{d}y\ . \end{aligned}$$

Implementing the step function in the initial condition in Equation (2.2.33), we have

$$\begin{aligned} a_{0,m} &= \frac{1}{2L^2}\left[\int_{-L}^{-a}\int_{-L}^{L}\cos\left(\frac{m\pi}{L}y\right)\,\mathrm{d}x\,\mathrm{d}y+\int_{-a}^{a}\int_{-L}^{-a}\cos\left(\frac{m\pi}{L}y\right)\,\mathrm{d}x\,\mathrm{d}y\right.\\ &\quad\left.+\int_{-a}^{a}\int_{-a}^{a}0\,\mathrm{d}x\,\mathrm{d}y+\int_{a}^{L}\int_{-L}^{L}\cos\left(\frac{m\pi}{L}y\right)\,\mathrm{d}x\,\mathrm{d}y+\int_{-a}^{a}\int_{a}^{L}\cos\left(\frac{m\pi}{L}y\right)\,\mathrm{d}x\,\mathrm{d}y\right]\\ a_{0,m} &= -\frac{2a}{m\pi L}\sin\left(\frac{m\pi}{L}a\right)\ . \end{aligned}$$

Also, to get $a_{n,m}$, we multiply each term of Equation (2.2.34) by $\cos\left(\frac{n\pi}{L}x\right)$ and $\cos\left(\frac{m\pi}{L}y\right)$, and then integrate over the square $([-L,L]\times[-L,L])$,

$$\begin{aligned} &\int_{-L}^{L}\int_{-L}^{L}a_{0,0}\cos\left(\frac{n\pi}{L}x\right)\cos\left(\frac{m\pi}{L}y\right)\,\mathrm{d}x\,\mathrm{d}y+\sum_{n\geq 1}a_{n,0}\int_{-L}^{L}\int_{-L}^{L}\cos\left(\frac{m\pi}{L}y\right)\cos^2\left(\frac{n\pi}{L}x\right)\,\mathrm{d}x\,\mathrm{d}y\\ &\quad+\sum_{m\geq 1}a_{0,m}\int_{-L}^{L}\int_{-L}^{L}\cos\left(\frac{n\pi}{L}x\right)\cos^2\left(\frac{m\pi}{L}y\right)\,\mathrm{d}x\,\mathrm{d}y\\ &\quad+\sum_{n\geq 1}\sum_{m\geq 1}a_{n,m}\int_{-L}^{L}\int_{-L}^{L}\cos^2\left(\frac{n\pi}{L}x\right)\cos^2\left(\frac{m\pi}{L}y\right)\,\mathrm{d}x\,\mathrm{d}y\\ &\quad=\int_{-L}^{L}\int_{-L}^{L}\phi(x,y)\cos\left(\frac{n\pi}{L}x\right)\cos\left(\frac{m\pi}{L}y\right)\,\mathrm{d}x\,\mathrm{d}y\ . \end{aligned}\tag{2.2.39}$$

Using the results in Equation (2.2.36),

$$a_{n,m} = \frac{1}{L^2}\int_{-L}^{L}\int_{-L}^{L} \phi(x,y)\,\cos\left(\frac{n\pi}{L}x\right)\cos\left(\frac{m\pi}{L}y\right)\,\mathrm{d}x\,\mathrm{d}y\ .$$

Implementing the step function in the initial condition in Equation (2.2.33),

$$a_{n,m} = -\frac{4}{nm\pi^2}\sin\left(\frac{n\pi}{L}a\right)\sin\left(\frac{m\pi}{L}a\right)\ .$$

Substituting the values of $a_{0,0}$, $a_{n,0}$, $a_{0,m}$, and $a_{n,m}$ into Equation (2.2.32), we have

$$\begin{aligned} u(x,y,t) = &\left(1-\frac{a^2}{L^2}\right) - \frac{2a}{L}\sum_{n\geq 1}\frac{1}{n\pi}\sin\left(\frac{n\pi}{L}a\right)\cos\left(\frac{n\pi}{L}x\right)e^{-D\frac{\pi^2}{L^2}n^2t} \\ &- \frac{2a}{L}\sum_{m\geq 1}\frac{1}{m\pi}\sin\left(\frac{m\pi}{L}a\right)\cos\left(\frac{m\pi}{L}y\right)e^{-D\frac{\pi^2}{L^2}m^2t} \\ &- 4\sum_{n\geq 1}\sum_{m\geq 1}\frac{1}{nm\pi^2}\sin\left(\frac{n\pi}{L}a\right)\sin\left(\frac{m\pi}{L}a\right)\cos\left(\frac{n\pi}{L}x\right)\cos\left(\frac{m\pi}{L}y\right)e^{-D\frac{\pi^2}{L^2}(n^2+m^2)t}\ . \end{aligned} \tag{2.2.40}$$

We integrate the function $u(x,y,t)$ as defined in Equation (2.2.40) over the bleach region ($([-a,a]\times[-a,a])$)

$$\begin{aligned} H(t,D) = &\int_{-a}^{a}\int_{-a}^{a}\left(1-\frac{a^2}{L^2}\right)\mathrm{d}x\,\mathrm{d}y - \frac{2a}{L}\sum_{n\geq 1}\frac{1}{n\pi}\sin\left(\frac{n\pi}{L}a\right)e^{-D\frac{\pi^2}{L^2}n^2t}\int_{-a}^{a}\int_{-a}^{a}\cos\left(\frac{n\pi}{L}x\right)\,\mathrm{d}x\,\mathrm{d}y \\ &- \frac{2a}{L}\sum_{m\geq 1}\frac{1}{m\pi}\sin\left(\frac{m\pi}{L}a\right)e^{-D\frac{\pi^2}{L^2}m^2t}\int_{-a}^{a}\int_{-a}^{a}\cos\left(\frac{m\pi}{L}y\right)\,\mathrm{d}x\,\mathrm{d}y \\ &- 4\sum_{n\geq 1}\sum_{m\geq 1}\frac{1}{nm\pi^2}\sin\left(\frac{n\pi}{L}a\right)\sin\left(\frac{m\pi}{L}a\right)e^{-D\frac{\pi^2}{L^2}(n^2+m^2)t}\int_{-a}^{a}\int_{-a}^{a}\cos\left(\frac{n\pi}{L}x\right)\cos\left(\frac{m\pi}{L}y\right)\,\mathrm{d}x\,\mathrm{d}y \end{aligned}$$

$$\begin{aligned} H(t,D) = &4a^2\left(1-\frac{a^2}{L^2}\right) - \frac{8a^2}{\pi^2}\sum_{n\geq 1}\frac{1}{n^2}\sin^2\left(\frac{n\pi}{L}a\right)e^{-D\frac{\pi^2}{L^2}n^2t} - \frac{8a^2}{\pi^2}\sum_{m\geq 1}\frac{1}{m^2}\sin^2\left(\frac{m\pi}{L}a\right)e^{-D\frac{\pi^2}{L^2}m^2t} \\ &- \frac{16L^2}{\pi^4}\sum_{n\geq 1}\sum_{m\geq 1}\frac{1}{n^2m^2}\sin^2\left(\frac{n\pi}{L}a\right)\sin^2\left(\frac{m\pi}{L}a\right)e^{-D\frac{\pi^2}{L^2}(n^2+m^2)t}\ . \end{aligned}$$

Since $L_c = 2L$ and $L_b = 2a$, we have

$$\begin{aligned} H(t,D) = &L_b^2\left(1-\frac{L_b^2}{L_c^2}\right) - \frac{2L_b^2}{\pi^2}\sum_{n\geq 1}\frac{1}{n^2}\sin^2\left(\frac{n\pi L_b}{L_c}\right)e^{-4D\frac{\pi^2}{L_c^2}n^2t} \\ &- \frac{2L_b^2}{\pi^2}\sum_{m\geq 1}\frac{1}{m^2}\sin^2\left(\frac{m\pi L_b}{L_c}\right)e^{-4D\frac{\pi^2}{L_c^2}m^2t} \\ &- \frac{4L_c^2}{\pi^4}\sum_{n\geq 1}\sum_{m\geq 1}\frac{1}{n^2m^2}\sin^2\left(\frac{n\pi L_b}{L_c}\right)\sin^2\left(\frac{m\pi L_b}{L_c}\right)e^{-4D\frac{\pi^2}{L_c^2}(n^2+m^2)t} \end{aligned} \tag{2.2.41}$$

where L_c is the length of each side of the cell surface, L_b is the length of each side of the bleach region and D is the diffusion coefficient of the proteins.

This is the model for the square bleach spot.

3. FRAP analysis with different models

In this chapter, we analyse FRAP experiments using the models we developed. We used these models to simulate a typical FRAP recovery curve and then used the least square method to estimate the simulated diffusion coefficient from the data generated. We also analysed the effect of noise and immobile fraction on our ability to fit the diffusion coefficient accurately.

3.1 Description of the models

3.1.1 One dimensional models. We begin by describing the one-dimensional models which are reasonable approximations of bleaching a rectangular strip. These models were developed by using the one-dimensional diffusion equation given in Equation (2.1.1). In developing the one-dimensional models, this equation was solved using two different approaches which are the Fourier transforms and Fourier series approach. The Fourier transforms method assumes the cell surface is infinite while the Fourier Series method assumes it is finite.

For the Fourier transform method, we considered a bleach region of width w_b and as initial condition, we assumed that the initial fluorescence intensity is unity everywhere on the strip except in the bleached region where it is zero as a result of the bleaching. In order to obtain our model, we integrated the solution of the diffusion equation over the entire bleached region. The model for this method is given as

$$H(t,D) = \frac{2\sqrt{Dt}}{\sqrt{\pi}}\left[1 - \exp\left(\frac{-w_b^2}{4Dt}\right)\right] + w_b\left[\operatorname{erf}\left(\frac{w_b}{2\sqrt{Dt}}\right) - 1\right] \tag{3.1.1}$$

where erf is the usual error function, D is the diffusion coefficient of the proteins and w_b is the width of the bleached region.

(See chapter two for detailed derivation of the model.)

In deriving the Fourier series model, we assumed that the cell has a length L_c and a bleach region of width w_b. We used the same initial condition as that of the Fourier transforms approach and then solved the diffusion equation in Equation (2.1.1) using the method of separation of variables and Fourier series method. The solution obtained was integrated over the bleached region to obtain our model. The Fourier series model is,

$$H(t,D) = w_b\left(1 - \frac{w_b}{L_c}\right) - \frac{2L_c}{\pi^2}\sum_{n\geq 1}\frac{1}{n^2}\sin^2\left(\frac{n\pi\, w_b}{L_c}\right)e^{-D\left(\frac{2n\pi}{L_c}\right)^2 t} \tag{3.1.2}$$

where L_c is the length of the cell, w_b is the width of the bleached region and D is the diffusion coefficient of the proteins.

(See chapter two for detailed derivation of the model.)

3.1.2 Two dimensional models. For this case, we considered the square bleach spot and the disc bleach spot. For a disc bleach spot, we used the diffusion equation in cylindrical coordinates to develop the model but assumed that there is no diffusion in the z-coordinate (Equation (2.2.1)). We assumed that the radius of the disc is a and that the cell surface is infinite. We also assumed the fluorescence intensity on the boundary of the disc is unity at all time and that the initial intensity in the interior

part of the disc is zero, simulating the bleached region. We solved the diffusion equation in Equation (2.2.1) with these initial and boundary conditions and assumed that there is symmetry in the diffusion of fluorescence on the disc. The solution of the diffusion equation was integrated over the entire bleached region in order to obtain our model. The model is given as

$$H(t,D) = a^2\pi - \sum_{i=0}^{\infty} \frac{4\pi}{\alpha_i^2}\, e^{-\alpha_i^2 Dt} \tag{3.1.3}$$

where a is the radius of the disc and α_i is the i^{th} zero of the Bessel function of the first kind of order zero.

(See chapter two for detailed derivation of the model.)

In modelling a FRAP experiment with a square bleach spot, we used the two-dimensional diffusion equation in xy coordinates given in Equation (2.2.20). We assumed the surface of the cell is a square of sides L_c and that the bleached region is a smaller square of sides L_b on the surface of the cell (See Figure 2.3).

In addition to this, we assumed that the fluorescence intensity everywhere on the cell surface is unity except in the bleached region (smaller square) where the intensity is zero. We solved the diffusion equation in Equation (2.2.20) using separation of variables and Fourier series method and then integrate the solution over the entire bleach region. Our model in this case is given as

$$\begin{aligned} H(t,D) = L_b^2\left(1-\frac{L_b^2}{L_c^2}\right) &- \frac{2L_b^2}{\pi^2}\sum_{n\geq 1}\frac{1}{n^2}\sin^2\left(\frac{n\pi L_b}{L_c}\right) e^{-4D\frac{\pi^2}{L_c^2}n^2 t} \\ &- \frac{2L_b^2}{\pi^2}\sum_{m\geq 1}\frac{1}{m^2}\sin^2\left(\frac{m\pi L_b}{L_c}\right) e^{-4D\frac{\pi^2}{L_c^2}m^2 t} \\ &- \frac{4L_c^2}{\pi^4}\sum_{n\geq 1}\sum_{m\geq 1}\frac{1}{n^2m^2}\sin^2\left(\frac{n\pi L_b}{L_c}\right)\sin^2\left(\frac{m\pi L_b}{L_c}\right) e^{-4D\frac{\pi^2}{L_c^2}\left(n^2+m^2\right)t} \end{aligned} \tag{3.1.4}$$

where L_c is the length of each side of the cell, L_b is the length of each side of the bleach region and D is the diffusion coefficient of the proteins.

(See chapter two for detailed derivation of the model.)

3.2 FRAP simulations

In this sections, we used the models developed to simulate FRAP recovery curves and then used the least square method to fit the diffusion coefficient from the generated data. All simulation were carried out using Sage. We evaluated our models at different time points with a known value of diffusion coefficient over a specified time interval. The value of these models at each time point gives the fluorescence intensity in the bleached region at the specified time. The data generated were used to simulate FRAP curves. Figures 3.1 shows the data generated using the one-dimensional Fourier transforms and Fourier series models. We considered a bleached region of $2\,\mu m$ for these models and for the Fourier series model, we assumed a cell of length $10\,\mu m$.

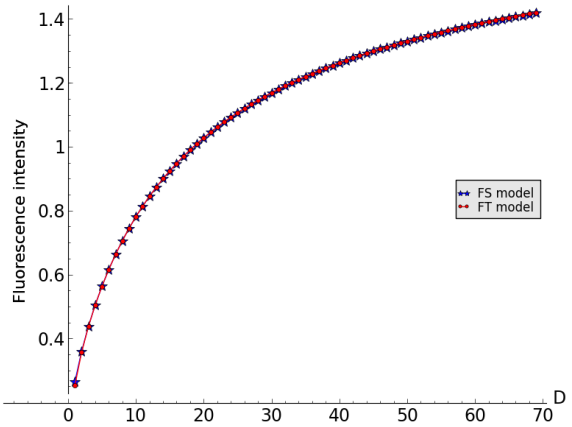

Figure 3.1: Simulated FRAP recovery curves using the 1D models.

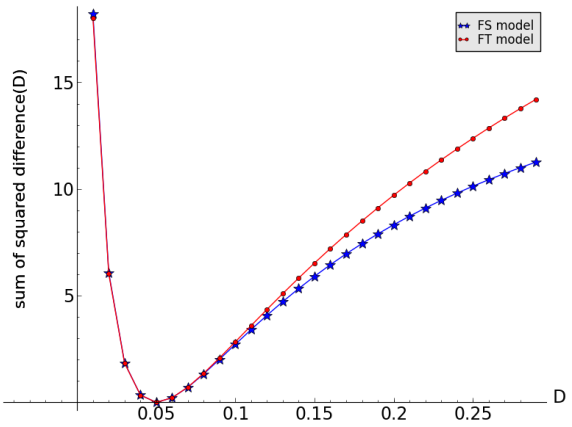

Figure 3.2: Fitting the diffusion coefficient using simulated data in Figure 3.1

In generating these FRAP curves, we considered 70 time points at 1 Hz, a diffusion coefficient of $D = 0.05\ \mu m/s$ and mobile fraction $M_f = 1$ (which means that we have 100% recovery). The 1D models predict the same fluorescence intensity in the bleached regions except at the few time points. After simulating the curves, we used the least square method to estimate the diffusion coefficient from the data. We were able to estimate D accurately from the generated data (See Figures 3.2).

For the disc bleach spot, we used the model in Equation (3.1.3) and considered a disc of radius 1, 70 time points, $D = 0.05\,\mu m^2/s$ and $M_f = 1$ (Figure 3.3). We were also able to recover the diffusion coefficient from the generated data accurately (Figure 3.4). The simulated FRAP curve for the square bleach spot is displayed in Figure 3.5. This curve was generated using the model in Equation (3.1.4), and considering a cell surface area of $100\,\mu m^2$. It is recommended that the bleached region should be located at the center of the cell and that it should be less than 5% of the total surface area of the cell in order to estimate the diffusion coefficient as accurate as possible (Dushek and Coombs, 2008). In accordance with this, we chose a bleach region of $4\,\mu m^2$ located at the center of the cell (See Figure 2.3 for example). In this case, we also considered 70 data points, $D = 0.05\,\mu m^2/s$ and $M_f = 1$. Then we used the least square method to fit the diffusion coefficient from the simulated data (Figure 3.6).

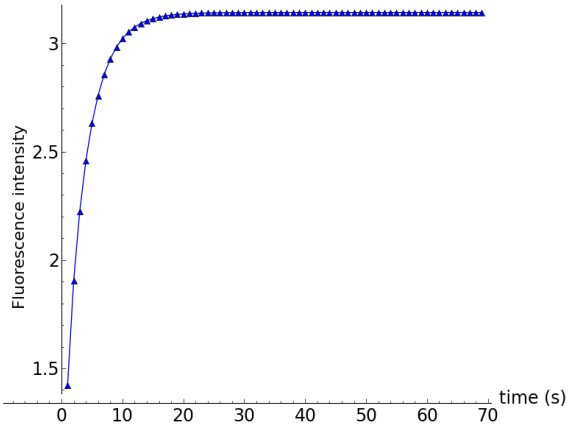

Figure 3.3: Simulated FRAP recovery curve generated using the model in Equation (3.1.3).

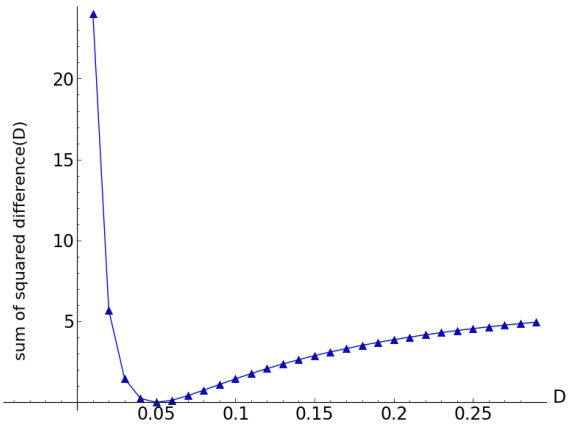

Figure 3.4: Fitting the diffusion coefficient using simulated data in Figure 3.3.

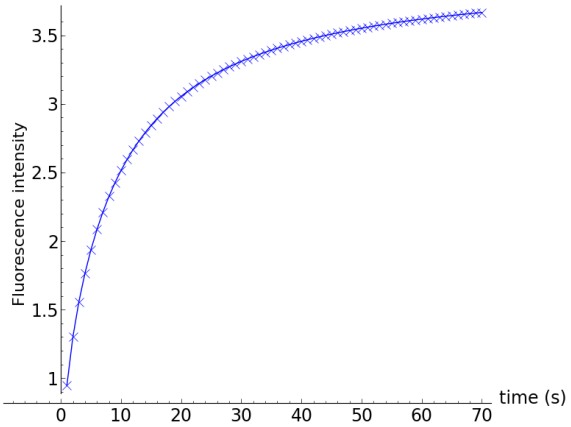

Figure 3.5: Simulated FRAP recovery curve generated using the model in Equation (3.1.4).

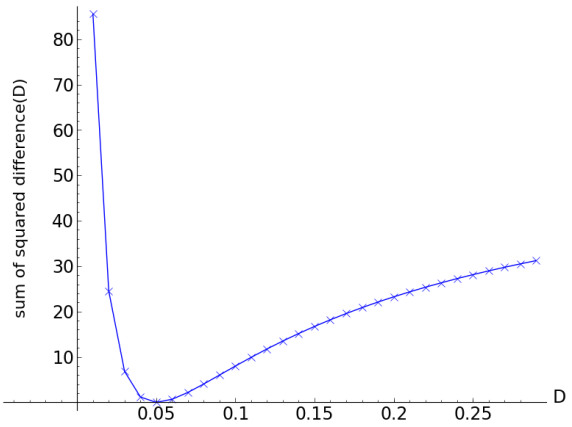

Figure 3.6: Fitting the diffusion coefficient using simulated data in Figure 3.5.

Next, we investigate the effect of noise on our ability to estimate the diffusion coefficient. To do this, we generated FRAP data with 15% gaussian noise and tried to fit the diffusion coefficient from the noisy data. Figure 3.7 shows an example of a noisy data from FRAP experiment. For this case, the 1D models estimated the diffusion coefficient as $0.05\,\mu m/s$ (Figure 3.8) while the 2D models estimated it as $0.06\,\mu m^2/s$ with an error of 20% (Figure 3.9 and Figure 3.10) .

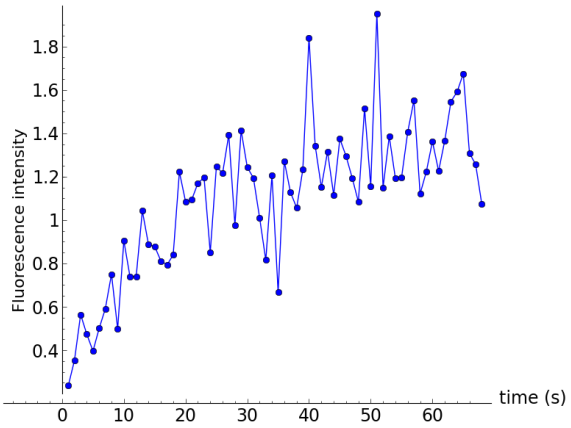

Figure 3.7: Simulated data with 15% gaussian noise.

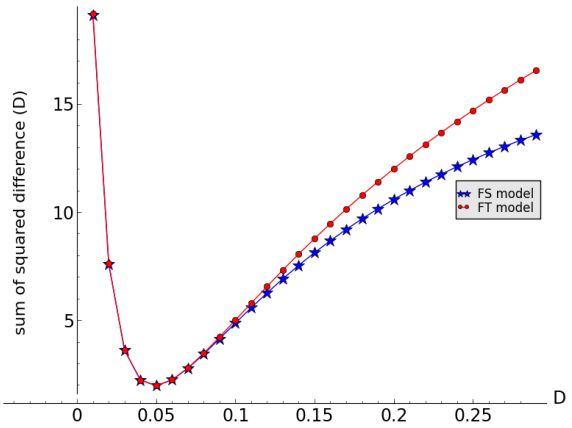

Figure 3.8: Fitting the diffusion coefficient from data with 15% noise using the 1D models.

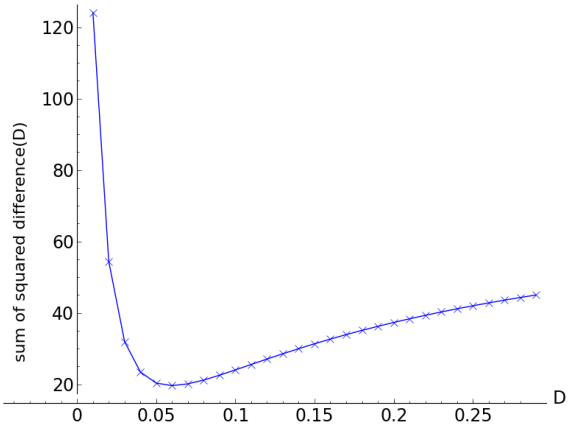

Figure 3.9: Fitting the diffusion coefficient from data simulated with 15% noise using the model in Equation (3.1.4).

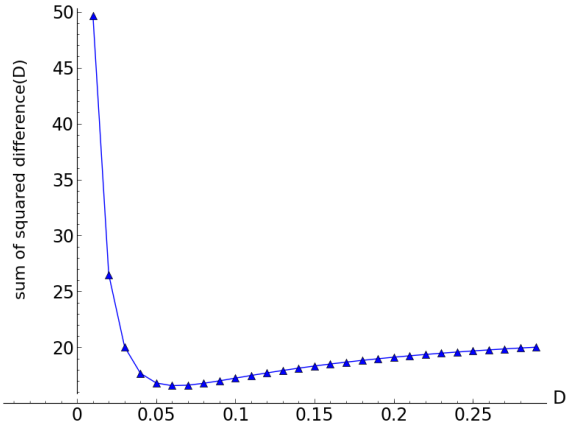

Figure 3.10: Fitting the diffusion coefficient from data simulated with 15% noise using the model in Equation (3.1.3).

Figure 3.11 and 3.12 show a 95% confidence interval test on estimating the diffusion coefficient of proteins from simulated data with different variances of noise for the 1D and 2D model respectively. In these figures, $\overline{x}$ is the mean fit of the diffusion coefficient and σ is the standard deviation of the fits. For each level of noise, we simulated data and fit the diffusion coefficient with the generated data. We repeat this process 100 times for each level of noise and then calculate the mean fit $(\overline{x})$ and standard deviation (σ).

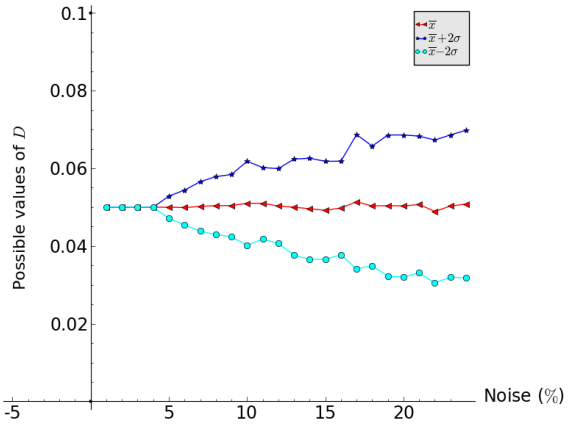

Figure 3.11: Estimate of D for 1D models (95% confidence interval).

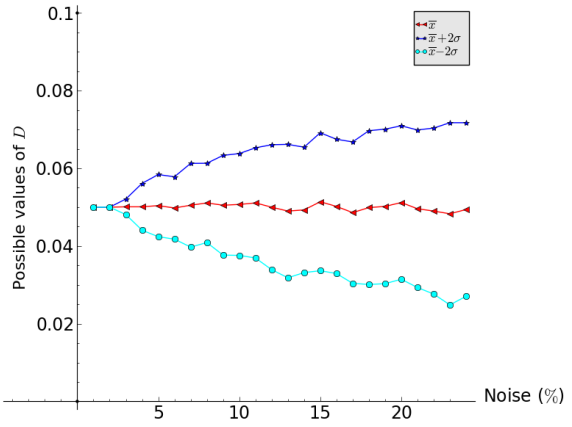

Figure 3.12: Estimate of D for 2D models (95% confidence interval).

We observed from Figure 3.11 that for the 1D models, at 95% confidence level, we can estimate the diffusion coefficient accurately for a noise level less than 5%, and with an error of at most 40% for data with 25% noise. While for the 2D models (Figure 3.12), we can estimate the diffusion coefficient with an error of at most 20% from data with 10% noise and with an error of at most 50% from data with 25% noise.

Since it is often difficult to have 100% fluorescence recovery during FRAP experiment, in addition to the effect of noise, we also investigated the effect of immobile fraction on our ability to fit the diffusion coefficient. We used data simulated with 15% gaussian noise and assumed that 5% of the proteins are immobile. In recovering the diffusion coefficient, the 1D models estimated D as $0.06\,\mu m/s$, the square bleach model estimated it as $0.06\,\mu m^2/s$ while the other 2D model estimated it as $0.07\,\mu m^2/s$ with 60% accuracy. These results are displayed in Figures 3.13 and 3.14 for the 1D models, Figure 3.16 for the square bleach model and Figure 3.15 for the disc bleach model.

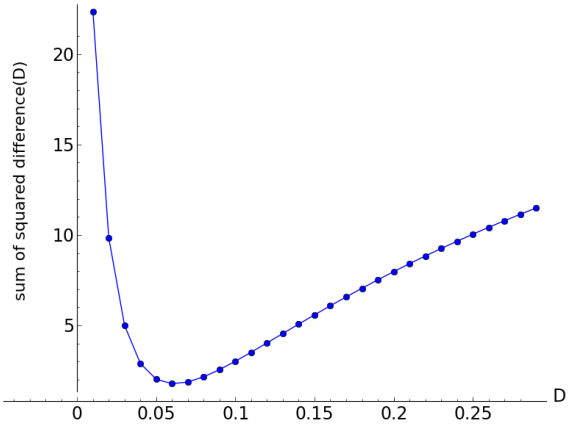

Figure 3.13: Fitting the diffusion coefficient from data simulated with 15% noise and 5% immobile fraction using the model in Equation (3.1.1).

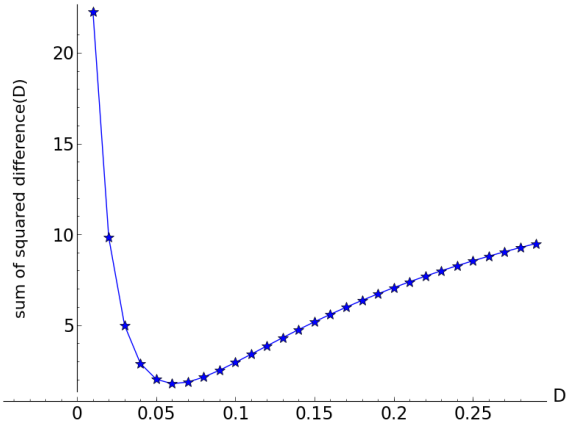

Figure 3.14: Fitting the diffusion coefficient from data simulated with 15% noise and 5% immobile fraction using the model in Equation (3.1.2).

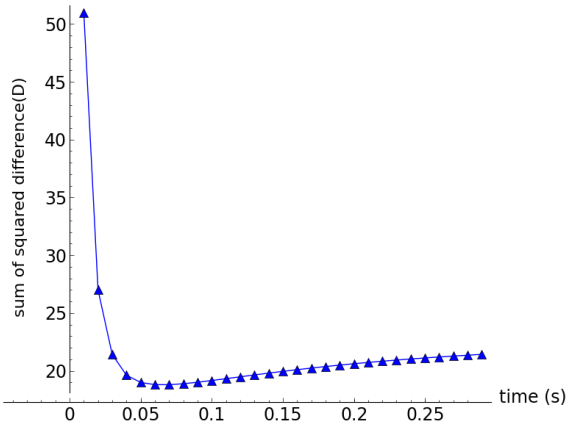

Figure 3.15: Fitting the diffusion coefficient from data simulated with 15% noise and 5% immobile fraction using the model in Equation (3.1.3).

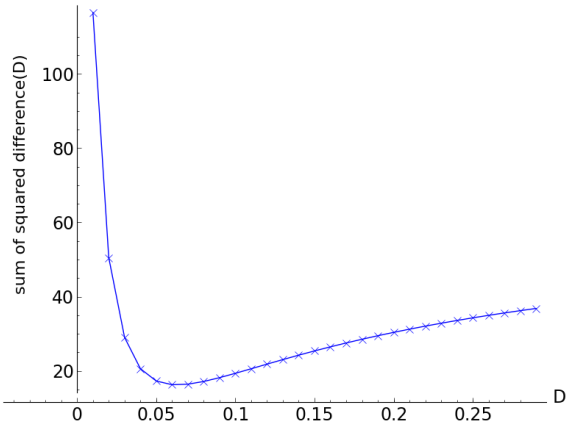

Figure 3.16: Fitting the diffusion coefficient from data simulated with 15% noise and 5% immobile fraction using the model in Equation (3.1.4).

4. Optimizing FRAP experiment

In this chapter, we optimize our ability to estimate the diffusion coefficient as accurate as possible either by acquiring data at specified locations in the bleached region during recovery or by acquiring the image of the entire bleached region at specified time points. This will help reduce the effect of the trade-off between the speed of data acquisition and the size of the bleached region, and also reduce the effect of background bleaching that occurs during data acquisition. All the investigations in the chapter are based on simulations and all simulations were carried out using Sage.

4.1 Optimizing spatial location for data acquisition

In this section, we optimize our ability to acquire data at a faster rate during FRAP experiment. Since the use the CLSM for FRAP experiment requires sequential scanning of the cell surface for data acquisition, we intend to acquire data only at specified locations of the bleached region in order the reduce the time taken to scan the entire bleached region and also to reduce the number of images acquired. This will help reduce the error in the data acquired as a result of the trade-off and background bleaching.

We considered the case of bleaching a rectangular strip, and simulated FRAP data using the 1D model in Equation (3.1.1). We partitioned the bleached region into equal sub-intervals and sampled fluorescence intensity in the region at period intervals instead of considering the entire region. These sampled intensities were used to estimate the average fluorescence intensity in the bleached region and also to fit the diffusion coefficient. We intend to find the optimal region for data sampling and also the optimal number of sub-intervals to be considered in order to estimate the diffusion coefficient as accurate as possible.

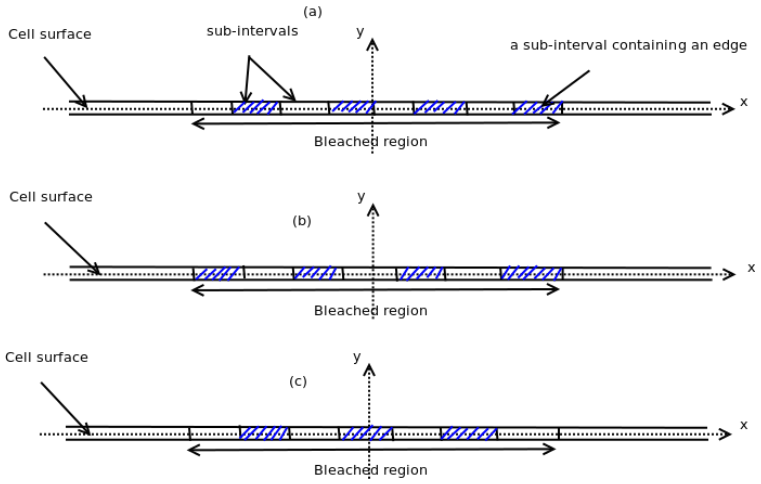

Figure 4.1: Partitioning the bleached region

Figure 4.1 shows the partitioning of a bleached region into equal sub-intervals. In this figure, every second sub-interval is selected and the selected sub-intervals are shaded in blue.

Since diffusion in this case is one-dimensional, we expect to have symmetry of fluorescence intensity about the middle of the bleached region with the highest intensity at the edges of the region. Therefore,

including the sub-intervals containing the two edges of the bleached region among the sampled sub-intervals will lead to over estimating the fluorescence intensity in the region. We carried out several experiments on this, considering different sizes of bleached region and different sub-intervals in the regions. Our experiment also shows that including the sub-intervals that contains the two edges of the bleached region among the sampled sub-intervals (Figure 4.1b) leads to over estimating the average fluorescence intensity in the region (except all the sub-intervals are considered), thereby giving a less accurate estimate of the diffusion coefficient. Including only one of the edges (See Figure 4.1a) gives a better estimate than including both.

In order to get the best estimate of the diffusion coefficient, the sampled intervals must exclude both edges of the bleached region. To achieve this, we partitioned the bleached region into sub-intervals and then select the sub-intervals in a periodic manner, such that non of the sub-intervals containing the edges are included in the selection (Figure 4.1c).

First, we considered selecting every second sub-interval, and then used the integrated fluorescence intensity in the intervals to predict the average fluorescence intensity in the bleached region. This average intensity is used to estimate the diffusion coefficient.

Next, we selected every third sub-intervals and then every fourth. Following the same procedure, the results obtained are similar. But the best estimate was obtained when every second sub-interval is selected as shown in Figure 4.1.

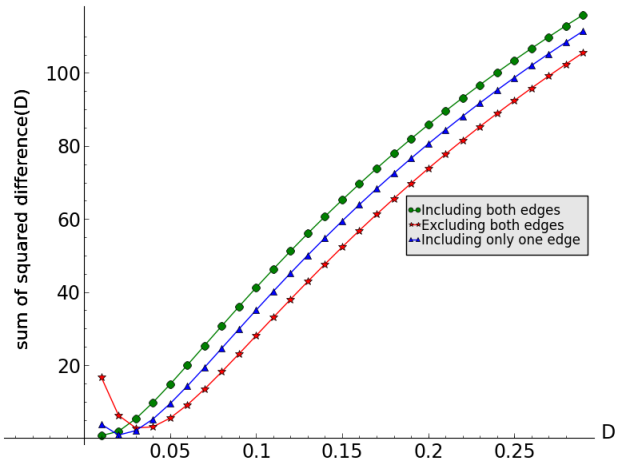

Figure 4.2: Fitting the diffusion coefficient by considering fluorescence intensity in different sub-intervals of the bleached region.

We initially carried out the investigation with data simulated without noise. Since a typical FRAP data contains noise, we simulated data with different variances of guassian noise and performed the same investigation. The results obtained in all cases are similar. Figure 4.2 shows the results of a particular case where different sub-intervals of the bleached region were considered. In this case, we considered a bleached region of width $4\mu m$, D=$0.05\mu m/s$, $M_f = 1$ and simulated data with 15% gaussian noise. In fitting the diffusion coefficient, we partitioned the bleached region into sub-intervals and considered different selections of the sub-intervals. When the sub-intervals containing the two edges of the bleached region were included in the sampling, the diffusion coefficient was estimated as $0.01\mu m$ with 80% error, and including only one of the edges, we obtained $0.02\mu m$, that is with 60% error. In the case where neither of the two edges was considered, the diffusion coefficient was estimated as $0.04\mu m$, with 20% error. We observed that the best estimate was obtained when neither of the two edges was included.

4.2 Optimizing the timing for data acquisition

In this section, we optimize the timing for data acquisition during FRAP experiment by acquiring fewer images during fluorescence recovery thereby reducing the amount of background bleaching that occurs during data acquisition.

For this investigation, we also considered bleaching a rectangular strip and assumed that we can acquire an image of the entire bleached region at once. We used the 1D models and considered different sizes of bleached region. The result are similar for both models and for all sizes of bleached region.

First, we simulated data without noise and considered fitting the diffusion coefficient from the data using only one time point and assuming $M_f = 1$. We were able to estimate the diffusion coefficient accurately irrespective of the time point considered. In addition to this, we considered using more than one time point and we were still able to estimate D accurately. In this case, the number of data points considered and the timing of the data does not affect the accuracy of the estimate. Next, we assumed there is an immobile fraction. In this situation, we were unable to estimate the diffusion coefficient accurately.

Furthermore, we simulated data with 15% gaussian noise and tried to fit the diffusion coefficient with few time points. We observed that considering only one time point, the point close to the beginning of fluorescence recovery give better estimate than others. And considering more than one time point, the points should be considerably spaced with more point at the beginning of the recovery. Also, at least two time points are required for estimates with high degree of accuracy (Figure 4.4). We varied the level of noise, and the results are similar for all noise variances.

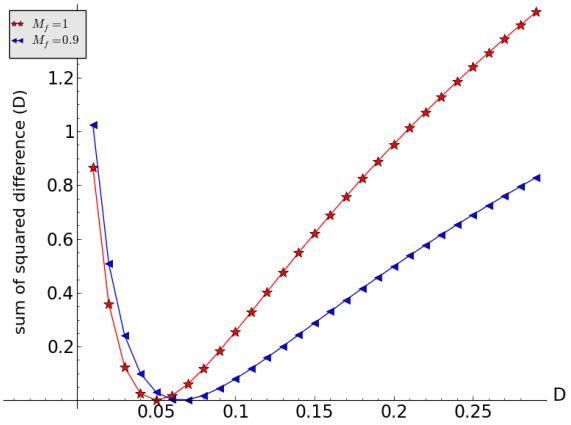

Figure 4.3: Fitting the diffusion coefficient using few time points (without noise).

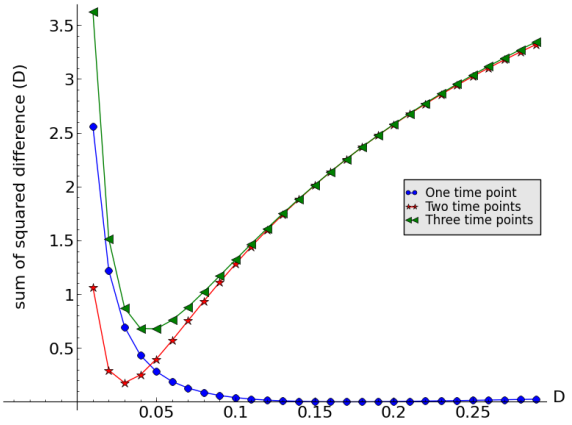

Figure 4.4: Fitting the diffusion coefficient using different numbers of time points.

Figure 4.3 shows a case where only two time points were considered for estimating D with $M_f = 1$ and the same time points were also used with $M_f = 0.9$. Figure 4.4 shows a case where different numbers of time points where considered. The data used in this case was simulated with 20% gaussian noise and $M_f = 1$. When we used only one time point, D was estimated as $0.19\mu m/s$, when we considered two time points, it was estimated as $0.03\mu m/s$ and with three time points, it was estimated as $0.04\mu m/s$.

5. Discussion and Conclusion

5.1 Discussion/Conclusion

We have developed several models for FRAP experiments with respect to different geometries of bleached region. We have 1D models for bleaching a rectangular strip, a model for a square bleach spot and another for a disc bleach spot. We used these models to simulate FRAP recovery curve and then used the least square method to fit the diffusion coefficient from the simulated data.

We have also analysed the effect of noise and immobile fraction on our ability to fit the diffusion coefficient accurately. We observed that with a noise level of 15%, we were able to estimate the diffusion coefficient accurately for the 1D models and with at least 80% accuracy for the 2D models. Also, with a 15% noise level and an immobile fraction of 5%, we were able to recover D with 80% accuracy for the 1D model and with at least 60% accuracy for the 2D models. This shows that noise and immobile fraction affects the accuracy of our fitting.

In addition, we investigated the robustness of the least square method as a technique for fitting diffusion coefficient from FRAP data. We carried out a 95% confidence interval test on this method using different variances of noise. For the 1D models, we estimated the diffusion coefficient accurately from simulated data with less than 5% noise and with an error of at most 40% from data with 25% noise. And for the 2D models, at 95% confidence level, we estimated the diffusion coefficient with an error of at most 20% from simulated data with 10% noise and at most 50% error for data with 25% noise.

Also, we provided a systematic way of sampling fluorescence intensity in the bleached region for 1D bleaching in order to reduce the effect of the trade-off between the speed of data acquisition and the size of the bleached region on the accuracy of the data acquired. This systematic sampling involves sampling fluorescence intensity in some selected sub-regions of the bleached region and then estimating the average intensity in the bleached region based on the sampled intensity. This technique will help reduce the time taken by the scanner to scan the entire bleached region. Using this approach, we observed that sampling fluorescence intensity at the two edges of the bleached region leads to over estimating the average intensity in the region and therefore, gives a less accurate estimate of D. And to get the best estimate of the diffusion coefficient, we must exclude sampling the fluorescence intensity at the two edges of the bleached region.

Furthermore, we provided a technique of reducing the noise in the data acquired during FRAP experiments as a result of background bleaching that occurs during image acquisition. This technique involves taking fewer images. We discovered that we can also estimate the diffusion coefficient with a high degree of accuracy by taking fewer images during fluorescence recovery. These images should not be acquired at consecutive time intervals, there should be a considerable time spacing between them with more images at the beginning of the recovery. Choosing the time of image acquisition carefully could be of benefit to the experimentalist.

5.2 Future work

Future work in this area may include further optimization of the locations and timing of data acquisition for 2D bleaching. In addition, the finite speed of the camera used in acquiring images may be explicitly included in the analysis.

Acknowledgements

My greatest thanks to Almighty God for the gift of life.

I would like to express my deep gratitude to my supervisor Professor Daniel Coombs for his valuable and constructive suggestions during the planning and development of this research work. And also, to my tutor Markus Kruger for his patience, guidance, enthusiatic encouragement and useful critiques of this research.

In addition, I would like to thank Dr. Sehun Chun for his assistance during this research and the entire AIMS family for their support during my studies at AIMS South Africa.

Finally, I wish to dedicate this project to my late parents and my siblings.

References

R. B. Adeniyi. *Basic essential topics in mathematical methods*. Evidence Nigeria Ventures, 2007.

D. Axelrod, D. E. Koppel, J. Schlessinger, E. Elson, and W. W. Webb. Mobility measurement by analysis of fluorescence photobleaching recovery kinetics. *Biophysical Journal*, 16:1055 – 1069, 1976.

K. Braeckmans, L. Peeters, N. N. Sanders, S. C. D. Smedt, and J. Demeester. Three-Dimensional fluorescence recovery after photobleaching with the confocal scanning laser microscope. *Biophysical Journal*, 85(4):2240–2252, 2003.

J. Braga, J. M. Desterro, and M. Carmo-Fonseca. Intracellular macromolecular mobility measured by fluorescence recovery after photobleaching with confocal laser scanning microscopes. *Journal of Biochemical and Biophysical Methods*, 15(10):4749–4760, 2004.

O. Dushek and D. Coombs. Improving parameter estimation for cell surface FRAP data. *Journal of Biochemical and Biophysical Methods*, 70(6):1224–1231, 2008. ISSN 0165-022X. doi: 10.1016/j.jbbm.2007.07.002. URL http://www.sciencedirect.com/science/article/pii/S0165022X07001443.

G. C. Everstine. *Analytic Solution of Partial Differential Equations*. 2012.

J. S. Goodwin and A. K. Kenworthy. Photobleaching approaches to investigate diffusional mobility and trafficking of ras in living cells. *Methods*, 37(2):154–164, 2005. ISSN 1046-2023. doi: 10.1016/j.ymeth.2005.05.013. URL http://www.sciencedirect.com/science/article/pii/S1046202305001301.

Mostinsky, I.L. Diffusion coefficient. Thermopedia, http://www.thermopedia.com/content/696/, Accessed April 2014.

Sage. *Sage Mathematics Software (Version 6.1)*. The Sage Development Team, 2014. URL http://www.sagemath.org.

Y. Sniekers and C. van Donkelaar. Determining diffusion coefficients in inhomogeneous tissues using fluorescence recovery after photobleaching. *Biophysical Journal*, 89(2):1302–1307, 2005. ISSN 0006-3495. doi: 10.1529/biophysj.104.053652. URL http://www.sciencedirect.com/science/article/pii/S0006349505727776.

Wikipedia (2014). Mass diffusivity. Wikipedia, the Free Encyclopedia, a. URL http://en.wikipedia.org/wiki/Mass_diffusivity.

Wikipedia (2014). Least squares. Wikipedia, the Free Encyclopedia, b. URL http://en.wikipedia.org/wiki/Leastsquare.